Asymmetric Geopotential Height Fluctuations from Symmetric Winds

MARK HOLZER

Canadian Centre for Climate Modelling and Analysis, Atmospheric Environment Service, University of Victoria, Victoria, British Columbia, Canada

(Manuscript received 23 December 1994, in final form 6 July 1995)

ABSTRACT

As a characterization of the variability of observed geopotential height fluctuations, their probability density function (PDF) and its skewness are studied in the global domain for winter and summer. The PDF of the geopotential, Φ, is skewed toward low anomalies at midlatitudes and toward high anomalies in polar and tropical regions. When Φ is filtered spatially by discarding planetary wavenumbers less than ~ 8, the skewness is small in the Tropics and in polar regions and large and negative in zonal bands approximately centered on the latitudes of the climatological jets. Where the skewness is large and negative, the zonally averaged PDF of Φ has an approximately exponential tail for negative anomalies.

From a diagnostic study based on computing Φ from the observed winds through the balance equation, the negative skewness bands can clearly be attributed to the rectification of near-symmetric velocity fluctuations by the advective nonlinearity. This mechanism implies that where winds are highly variable, large synoptic-scale negative Φ anomalies are more likely than large positive Φ anomalies. The maximum of the (negative) zonally averaged skewness in the summer hemisphere tends to be larger than that in the winter hemisphere, and in both hemispheres these maxima lie ~ 150 mb below the velocity variance maxima. The fact that skewness extrema do not precisely match maxima in the nonlinearities is attributed to asymmetries in the winds themselves. Interactions of the velocity fluctuations with the mean flow have a small but observable effect in modulating the skewness.

The subtle dependence of the skewness on key flow parameters is illustrated through an analytic model for idealized fluctuations on a beta plane. General expressions for the PDF, its asymptotic form, criteria for the presence of exponential tails, and the generic dependence of the skewness on a generalized Rossby number are derived. For the case of a δ-function velocity spectrum, closed-form expressions for the PDF and skewness are obtained and compared to observations.

1. Introduction

Atmospheric geopotential height fluctuations have a pronounced asymmetry. Especially at midlatitudes, large low anomalies (negative departures from the mean) in a given range of magnitudes are much more likely than high anomalies in the same range. This asymmetry is a basic characteristic of the field's variability that cannot be captured by an analysis of variance. A more complete characterization of the variability of geopotential, Φ, is its probability density function (PDF). Usually, however, there is insufficient data to estimate the PDF reliably at a point. Hence, we estimate what are essentially zonally averaged PDFs and quantify the local asymmetry of the geopotential height fluctuations by computing their skewness [the third moment of the (local) PDF, nondimensionalized by its variance]. Apart from its intrinsic interest as a basic characterization of the flow, a large skewness is usually also a signature of an underlying nonlinearity. White (1980) and, more recently, Nakamura and Wallace (1991) have studied the patterns of the skewness and kurtosis (nondimensionalized fourth moment of the PDF) of Northern Hemisphere (NH) 1000- and 500-mb low-frequency geopotential height fluctuations. These studies established a change of sign in skewness across the storm tracks, with positive skewness to the north and negative skewness to the south. Nakamura and Wallace (1991) speculate, with some empirical numerical evidence by Vautard et al. (1988), that the skewness comes from cutoff lows at the lower latitudes and from blocking anticyclones at high latitudes. No theory is available, however, to identify clearly the mechanism(s) that impart asymmetry to the low-frequency anomaly distribution, although baroclinic waves are strongly suspected to play a role (Nakamura and Wallace 1991; Vautard et al. 1988).

In this paper, we focus on both spatially filtered and unfiltered global geopotential fluctuations. For the filtered geopotential, Φ_{n_0}, obtained by discarding scales with planetary wavenumbers less than $n_0 \sim 8$, we can make a clean identification of the dominant mechanism

Corresponding author address: Dr. Mark Holzer, Canadian Centre for Climate Modelling and Analysis, Atmospheric Environment Service, University of Victoria, P.O. Box 1700, MS3339, Victoria, BC, Canada V8W 2Y2.

responsible for the skewness. The same mechanism is also responsible for most of the negative skewness on the large scales, although there asymmetry of the flow itself must be invoked to account for the remaining, mostly positive skewness. The PDF of geopotential fluctuations Φ', $P(\Phi')$, as computed from standard observational analysis or from general circulation model (GCM) output, is significantly skewed toward negative anomalies at midlatitudes in both hemispheres (see Fig. 1, discussed more fully in section 2). The skewness has a strong zonal structure and where it is large and negative, $P(\Phi')$ (zonally averaged) has a pronounced, approximately exponential tail for negative fluctuations, that is, $P(\Phi') \sim \exp(-(\text{const})|\Phi'|)$. The skewness of Φ is not a small effect. For example, in the summer hemisphere, at midlatitudes, 200-mb height anomalies of three standard deviations below the mean are about 10–100 times more likely than the same-size anomaly of the opposite sign!

We will show that the asymmetry of Φ fluctuations can be understood as a simple consequence of the nonlinearities of the balance equation and that this mechanism is responsible for much of the negative skewness on all scales studied. It should be emphasized that the mechanism consists of symmetric, random velocity fluctuations being rectified into asymmetric fluctuations of Φ. The dominant large negative skewness bands do not arise from the prevalence of a particular flow structure such as cutoff lows, although such structures might well be responsible for the remaining "unexplained" skewness, especially on the large scales. The phenomenon studied here is similar to that discussed by Holzer and Siggia (1993, hereafter HS) for homogeneous, isotropic turbulence. However, atmospheric flow, while for our purposes simply two dimensional, has the additional complications of being subject to the Coriolis force and an inhomogeneous mean background flow, which lead to a more complicated and interesting structure of $P(\Phi')$.

For idealized Gaussian, homogeneous, isotropic velocity fluctuations on a beta plane, we obtain the general functional form of $P(\Phi')$ analytically and derive criteria for the presence of exponential tails and the generic dependence of its skewness on a generalized Rossby number. For the special case of velocity fluctuations concentrated on a narrow band of wavenumbers, $P(\Phi')$ can be obtained in closed form and this will serve as an instructive example of how the skewing effect of the nonlinearities is modulated by the linear geostrophic balance and interactions with the mean state. In spite of its extreme simplifications, this model does capture the gross features of the observed $P(\Phi')$ when the observed mean state of the atmosphere is used to provided the background flow for the model fluctuations.

A first-order scale analysis for synoptic-scale motion determines Φ as an instantaneous quadratic functional of the velocity through the balance equation (see, e.g., Haltiner and Williams 1980), which in pressure coordinates is

$$\nabla^2\Phi = -\nabla\cdot(\mathbf{v}\cdot\nabla)\mathbf{v} - \nabla\cdot(\mathbf{f}\times\mathbf{v}), \qquad (1)$$

where $\mathbf{v}$ is the nondivergent ($\nabla\cdot\mathbf{v} = 0$) part of the horizontal wind velocity, and $\mathbf{f} = (2\Omega\sin\phi)\mathbf{k}$ is the Coriolis parameter for latitude ϕ. Because of the inhomogeneities of the background flow, it is much easier to deal with a velocity that has a PDF of zero mean. We therefore separate $\mathbf{v}$ into its mean $\bar{\mathbf{v}}$ (representing a mean annual cycle, a time average, or an ensemble average, as appropriate), and its fluctuations about that mean, $\mathbf{v}' = \mathbf{v} - \bar{\mathbf{v}}$. The nonlinear term of the balance equation (1) then becomes

$$\nabla\cdot(\mathbf{v}\cdot\nabla)\mathbf{v} = (\partial_i v_j)(\partial_j v_i) = \partial_i\partial_j(v_j'v_i' + 2\bar{v}_j v_i' + \bar{v}_j\bar{v}_i), \qquad (2)$$

where we have introduced component notation for clarity [$\partial_i \equiv \partial/\partial x_i$, where (x_1, x_2) is the horizontal position; repeated indices are summed]. In this expression, terms that do not involve the fluctuating parts of the velocity contribute to the mean of Φ but have otherwise no effect on its PDF. Equation (2) shows that inhomogeneities in the mean state impart contributions to the nonlinearity $\nabla\cdot(\mathbf{v}\cdot\nabla)\mathbf{v}$, which are linear in the fluctuations and which will be shown to modulate the effect of the truly nonlinear fluctuations ($\mathbf{v}'\mathbf{v}'$).

To see the basic mechanism that skews the distribution of Φ'_{n_0}, consider a flow in which the statistics of $\mathbf{v}'$ are symmetric in the sense that they are invariant under $\mathbf{v}' \to -\mathbf{v}'$, or at least that all its triple correlations, and in particular the skewness of its one-point PDF, vanish. Then the PDF of any term linear in $\mathbf{v}'$ must also be symmetric, so that in the absence of nonlinearities in $\mathbf{v}'$, Φ'_{n_0} would have zero skewness. To illustrate that the nonlinear term in (2) does turn symmetric velocity fluctuations into skewed Φ fluctuations, consider the contribution, Φ_{NL}, of the nonlinear term to Φ, which may be written as

$$\nabla^2\Phi_{\mathrm{NL}} \equiv -(\partial_i v_j')(\partial_j v_i') = \frac{1}{2}\zeta'^2 - s'^2, \qquad (3)$$

where $\zeta' = \mathbf{k}\cdot\nabla\times\mathbf{v}'$ is the (fluctuating) vorticity and $s'_{ij} \equiv (\partial_i v_j' + \partial_j v_i')/2$ is the (fluctuating) rate of strain tensor ($s^2 \equiv s_{ij}s_{ji}$). The fluctuations of Φ_{NL} cannot be symmetric since the right-hand side (rhs) of (3) is invariant under $\mathbf{v}' \to -\mathbf{v}'$, so that positive and negative velocities, by assumption occurring with equal probability, contribute to Φ_{NL} fluctuations of the same sign. It is in this sense that a skewed distribution of Φ_{NL} arises from the nonlinear "rectification" of symmetric velocity fluctuations.

The asymmetry of the PDF of Φ_{NL} can also be argued from an analogy with electrostatics in which the right-hand side of (3) is equated to the negative of a charge density so that Φ_{NL} is formally equivalent to an electrostatic potential. In three-dimensional turbulent

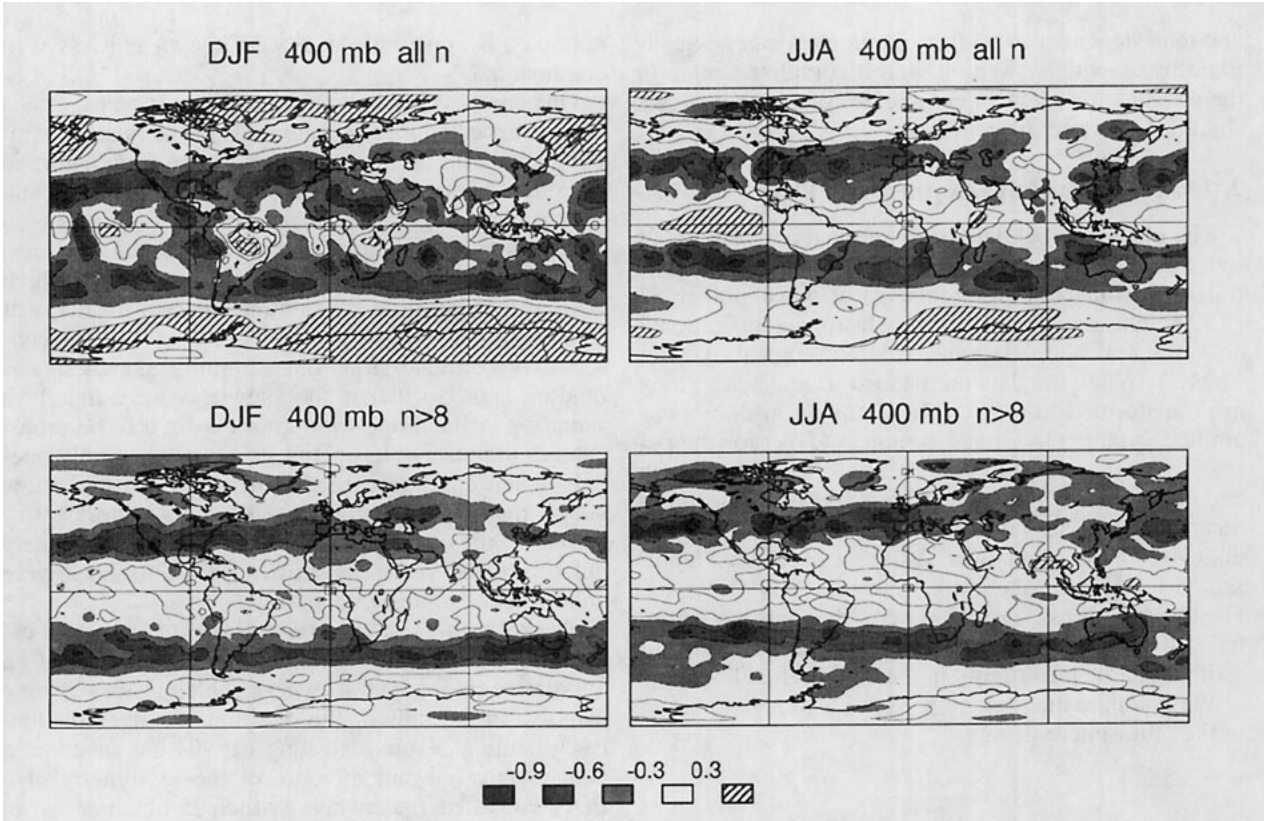

FIG. 1. Skewness of the unfiltered (all n) and filtered ($n > 8$) geopotential fluctuations, at 400 mb, where the skewness is approximately maximized. The contour interval is 0.3.

flows, vorticity tends to be localized (see, e.g., Siggia 1981), while the strain field is of a more extended nature (see, e.g., Brachet 1991), so that $-\zeta^2/2$ may be considered a collection of localized charges that locally sharply deform the Φ_{NL} surface, so that Φ_{NL} has larger negative than positive deviations from its mean. For a real turbulent geophysical flow, however, vorticity and strain structures are modified by strong stratification, and ζ^2 and s^2 are fluctuating and statistically dependent so that it is not a priori obvious what sign the skewness of Φ_{NL} has given a flow with an arbitrary spectrum. It turns out that for two-dimensional Gaussian, homogeneous, isotropic velocities the skewness of Φ_{NL} is negative definite for any spectrum (see HS and section 4). In section 4 we will see that even for such idealized fluctuations, the skewness of the full Φ is not necessarily negative, especially for small Rossby number.

On a more intuitive fluid mechanical level, the asymmetry of Φ_{NL} can be understood, for example, for a hypothetical strain-free, purely rotational flow. In that case, $\zeta^2/2$ represents the divergence of the centripital force that is always pointed toward the rotation center and hence independent of the sense of rotation, which is why it can only depend on ζ^2. Hence, such flow is always associated with a low (i.e., negative) anomaly independent of the direction of the flow so that symmetric vorticity fluctuations imply negatively skewed Φ_{NL} fluctuations. This "cyclostrophic" balance is to be contrasted with geostrophic balance where the direction of the Coriolis force does depend on the sign of ζ and whose divergence is $f\zeta$ (on an f plane). Thus, for geostrophic balance, symmetric fluctuations of ζ imply symmetric fluctuations of Φ.

The quadratic dependence of Φ on $\mathbf{v}$ suggests the asymptotic (i.e., large-Φ') form of $P(\Phi')$ by the following "back of the envelope" argument. Dimensionally, $\Phi \sim v^2$, so that if the velocity is Gaussian, that is, $P_v(v') \sim \exp[-(v'/v_0)^2]$, then $P(\Phi') \sim |\Phi'|^{-1/2} \times \exp(-|\Phi'|/v_0^2)$. By the same token, if the velocity itself were exponential, that is, $P_v(v') \sim \exp(-|v'/v_0|)$, then $P(\Phi')$ would be expected to be streched exponential, that is, $P(\Phi') \sim |\Phi'|^{-1/2} \exp(-|\Phi'|^{1/2}/v_0)$.

The full geopotential is given by the sum of Φ_{NL} and terms linear in the velocity fluctuations, which represent the interactions of the fluctuations with the mean state, and, of course, (linear) geostrophic balance. However, the PDF of Φ' is not simply the convolution of $P(\Phi'_{NL})$ and the PDF of the linear terms because these are, of course, not statistically independent. Nevertheless, when the nonlinear terms are strong (large Rossby number), we can expect asymmetries in $P(\Phi')$, while dominance of the linear terms implies a near-symmetric $P(\Phi')$. For the case of Gaussian velocities, the asymptotic form of $P(\Phi')$, its skewness,

and their dependence on flow parameters can be quantified by essentially writing Φ as a complete square in the statistically independent degrees of freedom as we shall demonstrate in section 4.

2. Observations of the skewness and PDF

The observational dataset in our analysis consists of twice daily, global fields for Φ and vorticity, ζ, in spectral form truncated (triangularly) at wavenumber 32 (T32). The data were derived from the operational analyses of the National Meteorological Center (NMC). When the data are needed in real space, they are transformed to a 96 × 48 Gaussian grid. We examined winters (DJF) and summers (JJA) for the period December 1978 to August 1988; for JJA we also had available an 8-yr set for 1984–1991. The more recent data are less noisy at the upper levels (higher than ~150 mb) and over Antarctica. Results represented for JJA are therefore from the 1984–1991 set. For the quantities considered here, there are no essential differences between the two sets that exceed our estimate of the uncertainty in the data (defined below).

We compute the skewness, S_Φ, of Φ at a given point in the atmosphere using

$$S_\Phi = \frac{\langle \Phi'^3 \rangle}{\langle \Phi'^2 \rangle^{3/2}}, \tag{4}$$

where $\Phi' \equiv \Phi - \bar{\Phi}$ represents the fluctuations of Φ about its mean annual cycle, $\bar{\Phi}$, and the brackets $\langle\ \rangle$ denote the average over the entire dataset for a given season, location, and level. For a given season, $\bar{\Phi}$ is estimated at every point in space as a least-squares fit of a parabola to the mean seasonal data (i.e., to Φ averaged over the years but not within a season). An independent fit for each year turns out to be inadequate because this systematically removes signal in regions of low variability such as the Tropics. Figure 1 shows S at 400 mb (chosen at the level where S is approximately maximized—see below) for Φ_0 and Φ_8 [i.e., Φ filtered to contain only planetary wavenumbers greater than 0 (unfiltered) and 8]. The skewness pattern observed for the unfiltered data is consistent with the NH analyses of White (1980) and Nakamura and Wallace (1991). Note the strong zonal structure in S so that it makes sense to consider the zonal average $[S]$, shown in Fig. 2a.

To get a rough estimate of the uncertainty in some quantity X, we split the time series of the data into two pieces of equal length. If X_1 and X_2 denote the values of X for each of the pieces, we take $|X_1 - X_2|/2$ as a measure of the uncertainty in X. This is what is plotted in Fig. 2b for the zonally averaged skewness ($X = [S]$). The large uncertainties found for DJF in the Southern Hemisphere (SH) south of ~60°S are due to well-known deficiencies in earlier NMC analysis (see, e.g., Trenberth and Olson 1988). The noisiness of the earlier data above ~100 mb, especially at higher wavenumbers, is apparently also well known but less well documented.

One can also ask how large $|S_\Phi|$ must be to exceed what is expected for the magnitude of the random sampling skewness of a finite sample drawn from a normal (zero true skewness) distribution. From the purely statistical considerations of the appendix, skewness may be considered statistically significant at the 5% level for our sample size if $|S_\Phi|$ exceeds about 0.3, which is what we choose as the contour interval for maps of S. It should be emphasized, however, that this is a conservative estimate. Random sampling skewness has random sign, so that if the skewness were merely a sampling artifact, one would not expect it to be robust enough to preserve its spatial structure when only one-half of the data are used. Furthermore, we will show below that a GCM produces skewness patterns very similar to the observations, which would be extremely unlikely if the skewness shown in Figs. 1 and 2 were an artifact of finite sample size.

The robustness of our straightforward skewness estimates can also be ascertained from the fact that an alternative measure of skewness, which is not sensitive to noise in the tails of the distribution, gives qualitatively similar results. Hosking (1990) has invented a conceptually elegant measure of the asymmetry of a PDF, so-called L-skewness, which is obtained as an appropriately normalized *linear* combination of ordered triplet statistics. The L-skewness differs numerically from the standard skewness due to the differences in definition. Nevertheless, for our dataset we find that the L-skewness is approximately a scaled version of the standard skewness and does not appear significantly less noisy. We therefore continue our analysis in terms of the conventional skewness as this is much easier to handle analytically and numerically.

The distinction of fluctuations about the mean annual cycle $\bar{\Phi}$ from fluctuations about the grand seasonal mean $\langle\Phi\rangle$ is only important for the large scales, especially for NH summer. Figure 2c shows $[S_\Phi]$ computed by replacing fluctuations about $\bar{\Phi}$ with fluctuations about $\langle\Phi\rangle$. Comparison with Fig. 2a (and Fig. 2b) shows that there are no significant differences except for the Northern Hemisphere during JJA, where the amplitude of the fluctuations of Φ are comparable to the amplitude of the quadratic seasonal trend, which can therefore enhance the skewness of the fluctuations about $\langle\Phi\rangle$.

Figures 1 and 2 show that Φ has large negative skewness in the general vicinity of the climatological jets. For the unfiltered data, the maxima of $|[S]|$ lie at the latitudes of the extrema of the zonally averaged vorticity equatorward of the jets, but at lower levels (~400 mb versus ~200 mb). This is again consistent with the observation of White (1980) and Nakamura and Wallace (1991) that the skewness of low-frequency anomalies changes sign across the storm tracks. As the large scales are discarded, the latitudes of the negative skew-

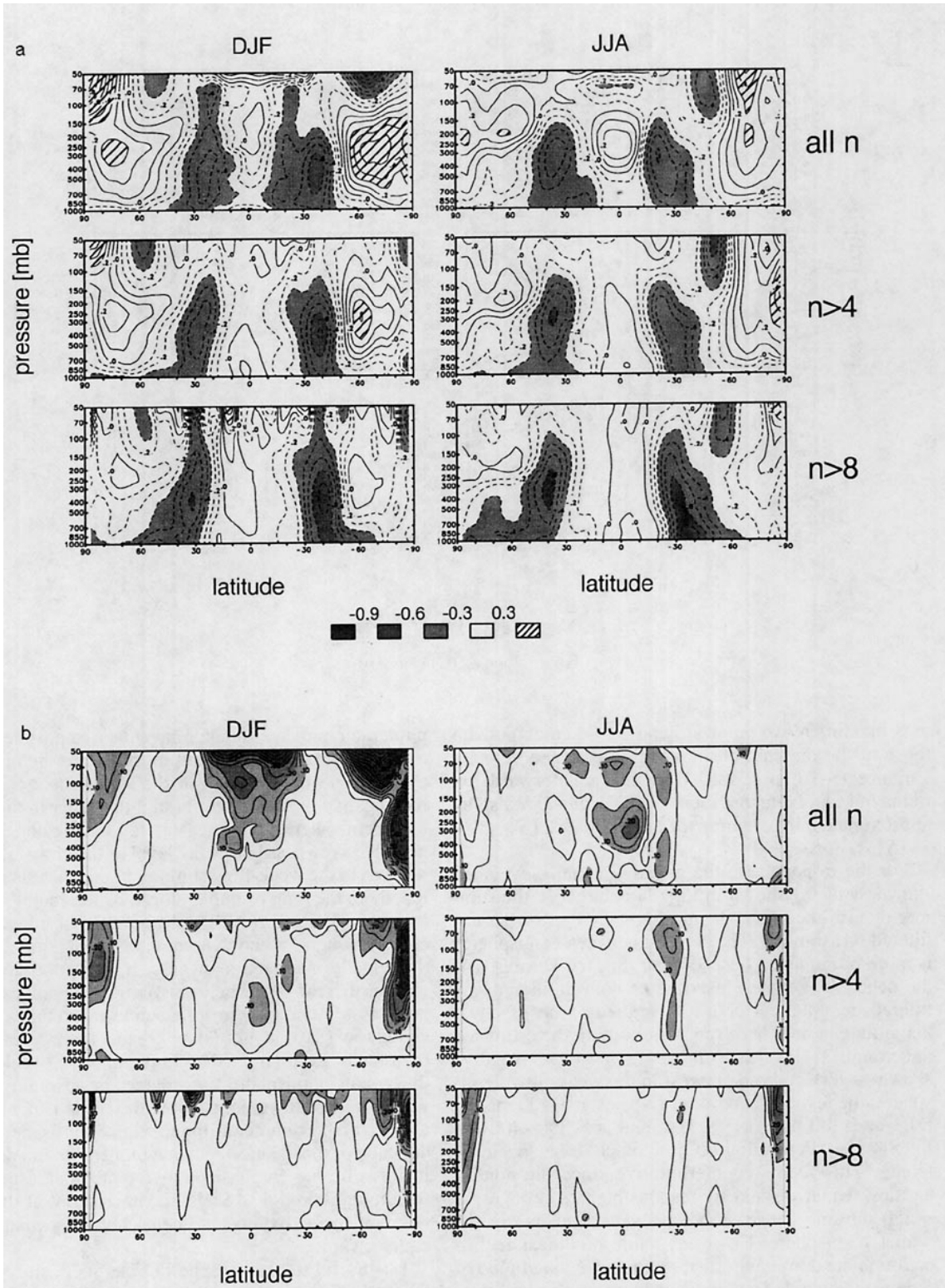

FIG. 2. (a) Zonal average of the skewness of the unfiltered and filtered fluctuations of geopotential about the mean parabolic seasonal trend $\bar{\Phi}$. The contour spacing is 0.1. (b) Estimate of the uncertainty in (a). The contour interval is 0.05 and values larger than 0.1 have been shaded. (c) Zonal average of the skewness of the fluctuations of geopotential about the grand seasonal mean $\langle\Phi\rangle$. The contour spacing is 0.1.

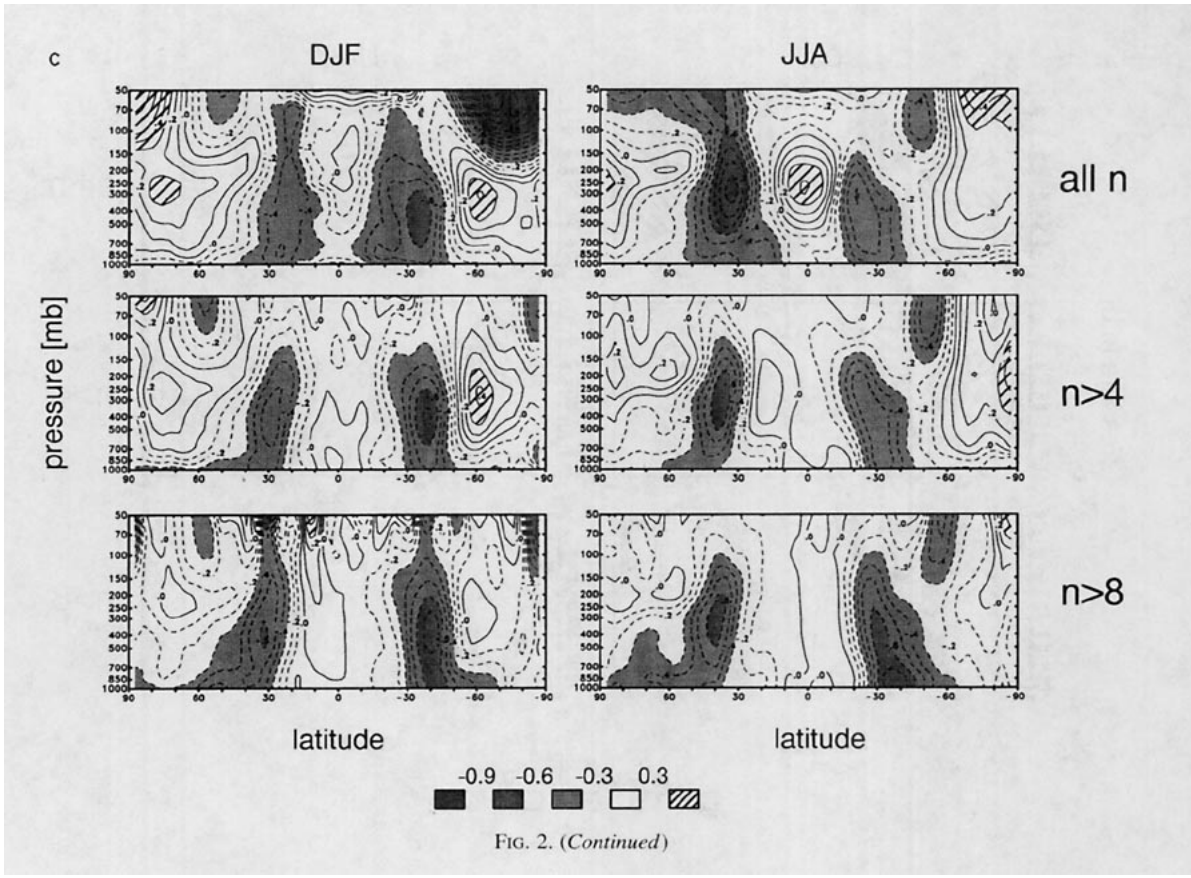

FIG. 2. (*Continued*)

ness maxima move poleward and for Φ_8 coincide with those of the maxima of the zonally averaged velocity variance ($\sim 10°$ poleward from the equatorward extrema of $[\zeta]$). Note that for $n \geq 4$, DJF and JJA display approximate mirror symmetry in $[S]$, that is, $[S]_{\mathrm{DJF}}(\phi) \sim [S]_{\mathrm{JJA}}(-\phi)$.

For the troposphere, the negative zonally averaged skewness of Φ_{n_0} shown in Fig. 2a is larger in the summer than in the winter hemisphere, except for the unfiltered NH summer. The contrast between hemispheres is more pronounced for DJF than for JJA. During JJA, the negative skewness maxima of both unfiltered and filtered geopotential could be argued to be of equal magnitude in both hemispheres to within the estimated uncertainties (Fig. 2b). In addition to the negative skewness tending to be largest in the weak-flow hemisphere, the level of maximum $|S|$ lies at $\sim$400 mb for DJF, at $\sim$300 mb for NH JJA, and at $\sim$300–400 mb for SH JJA (depending on how much Φ has been filtered). This seems counterintuitive since the nonlinearities, which we said are responsible, are strongest at $\sim$250 mb and (at least at low wavenumbers) in the winter hemisphere. However, while nonlinear rectification is the dominant effect, the precise magnitude of S depends on a delicate balance between its numerator and denominator.

Figure 3 shows the zonally averaged numerator and denominator of the skewness separately for Φ_4. Both numerator and denominator have their tropospheric extrema at $\sim$300–250 mb and in the winter hemisphere as one expects (although in the troposphere for DJF, the negative third moment is slightly larger in the summer hemisphere). The reason for having the largest negative skewness below the level of the climatological jets and in the weak-flow summer hemisphere is simply that there the ratio of numerator to denominator has the largest magnitude. (Although the ratio of zonally averaged numerator and denominator is not equivalent to the zonally averaged skewness, it is a good approximation thereof—see below.) A more negative skewness in the summer hemisphere does mean that a three-sigma low (say) is more likely than a three-sigma high by a factor even larger than in the high $|S|$ regions of the winter hemisphere. Of course, in absolute terms, three standard deviations below the mean is not nearly as deep in the summer as in the winter hemisphere. The delicacy of the balance between numerator and denominator is further emphasized by the fact that, especially for the unfiltered Φ, $|S|$ is maximized not at the latitudes of the individual moments but somewhat more equatorward.

It is useful to estimate the PDF as such, since just a few moments carry no information about its asymptotic form and do not uniquely determine its shape. We do not have enough data to estimate reliably the PDF at a point. Encouraged by the strong zonal structure of S,

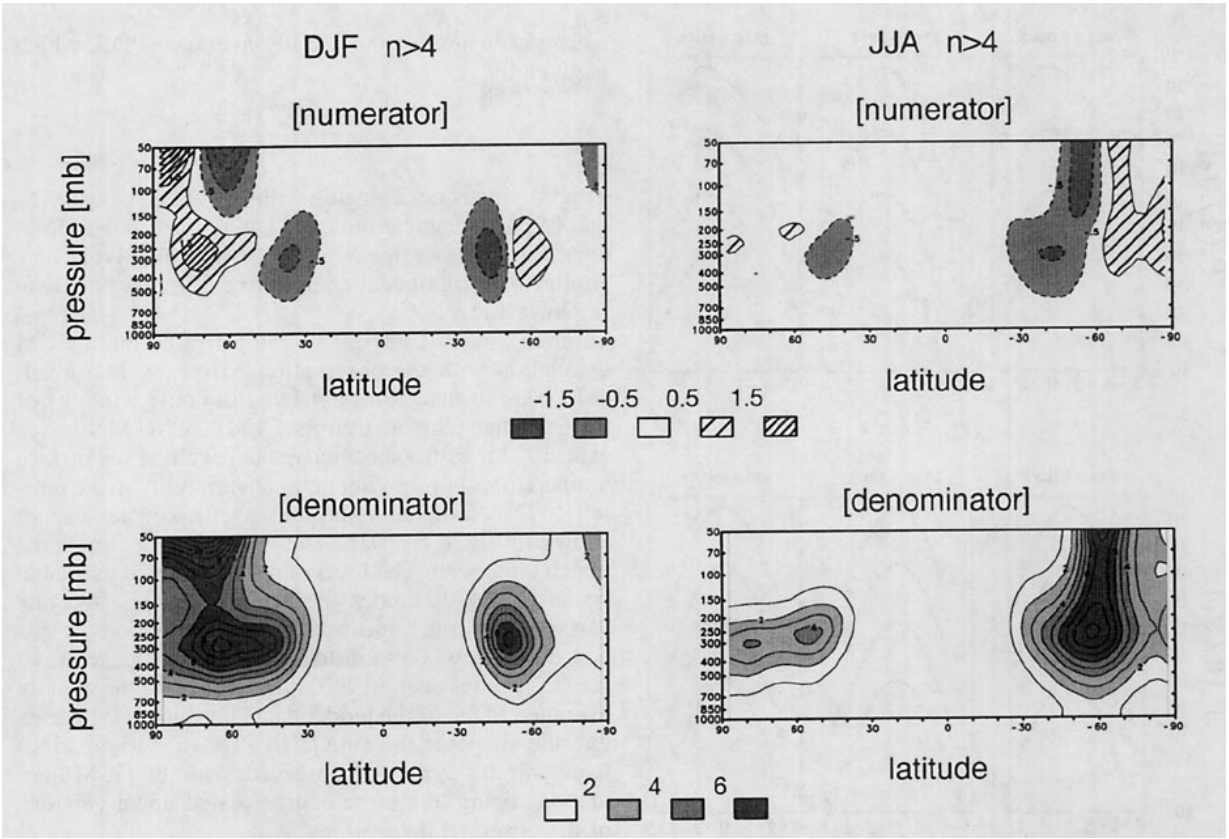

FIG. 3. Zonal averages of the numerator (top) and denominator (bottom) of the skewness of Φ_4. The units are arbitrary but the same for the numerator and denominator. The contour spacing is one unit.

we estimate, therefore, what is essentially the zonal average of $P(\Phi')$: in order to maximize the signal to noise ratio, we make a histogram of every value of Φ' on two adjacent grid latitudes for a given season and level. The normalized histogram thus approximates a PDF that is a zonal average of the PDFs for every grid point (and also meridionally averaged over two adjacent grid latitudes). Similarly, we also computed the corresponding PDFs of the zonal and meridional velocity fluctuations (about their annual cycle, estimated as for Φ), u' and v'. The results are shown in Fig. 4 at 400 mb for the equator and for latitudes chosen to coincide approximately with the maxima of $-[S]$.

The variances and skewnesses of the PDFs of Fig. 4 are collected in Table 1. For $n > 8$ the variances drop with a doubling of the filter cutoff n_0 in rough accordance with the expected exponent of the associated spectra. A power-law spectrum $\sim n^{-\alpha}$ implies a drop of the variance by a factor of $2^{\alpha-1}$ with a doubling of n_0. For the velocities, the exponents thus implied, for the three latitude bands shown, are (from N to S) $\alpha_v = 2.9 \pm 0.1, 2.5 \pm 0.3$, and 3.1 ± 0.3. The corresponding exponents for Φ are $\alpha_\Phi = 4.0 \pm 0.1, 3.8 \pm 0.6$, and 4.25 ± 0.05. The exponents of the computed global spectra (not shown) for the velocity and Φ are ~ 2.5 and ~ 4.5, respectively. The discrepancies between the exponents from the PDF variance and those of the global spectra and that $\alpha_\Phi - \alpha_v$ is significantly different from 2 are likely attributable to wavenumber 8 not quite lying in the power-law regime of the spectra.

Where the PDFs of Φ' are significantly skewed, there is a clear tail visible for negative anomalies that is decaying more slowly than a Gaussian. The tails are nearly exponential where they approximate a straight line on the semilog plot. For the Southern Hemisphere, for Φ_0, Φ_4, and Φ_8, the tail appears to have a kink at ~ -3 standard deviations, beyond which the PDF decays more rapidly. Although the error bars there, again estimated by splitting the data into two pieces, are nominally small, values below -3 standard deviations represent only $\sim 1\%$ of the data. Furthermore, it may be questionable whether Southern Hemisphere analysis is reliable enough to capture extreme events with fidelity.

For the velocity PDFs, the most important thing to appreciate is that they are approximately symmetric and that where asymmetries occur, they are lessened by discarding the large scales. Where Φ has $O(1)$ negative skewness, the skewnesses of u and v are at least an order of magnitude smaller. The u-component is close to Gaussian, while the PDF of v has more expo-

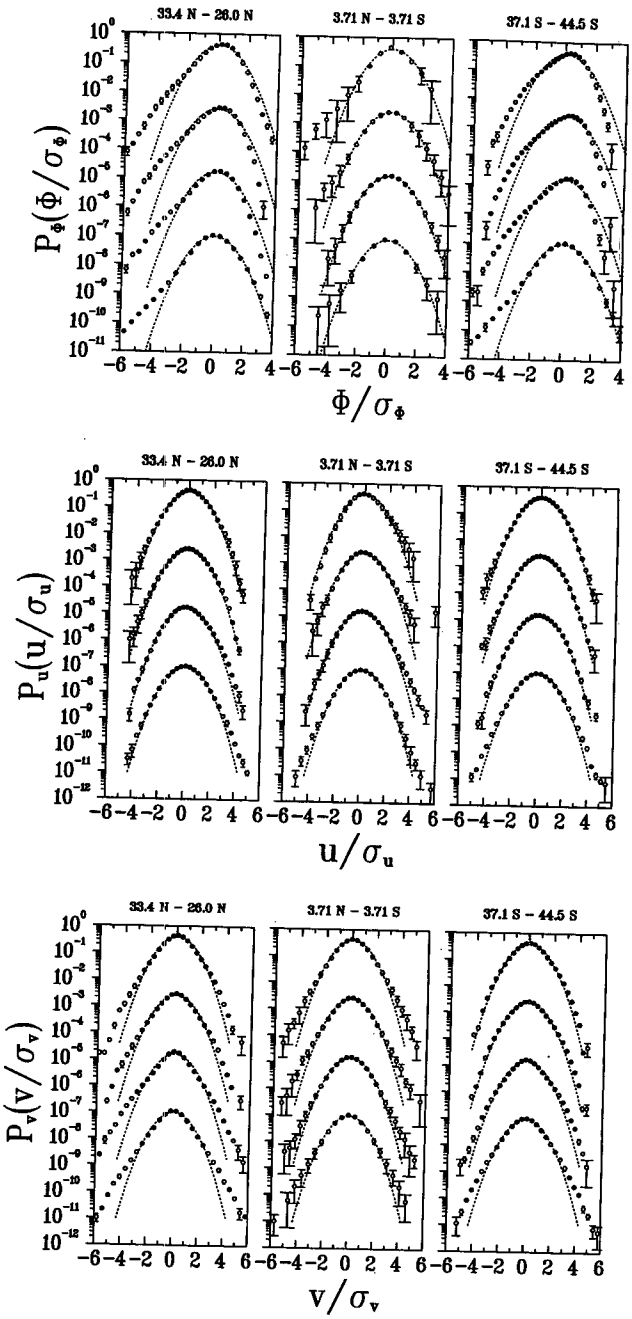

FIG. 4. Zonally averaged PDFs for Φ, u, and v at 400 mb, DJF for the latitude belts indicated. The PDFs are normalized to unit variance, shifted horizontally to zero mean, and shifted in the vertical for clarity. The PDFs, in order from top to bottom, are for the unfiltered field, for $n > 4$, $n > 8$, and $n > 16$. The dashed lines are unit-variance Gaussians for reference. (The standard deviation of variable x is denoted by σ_x.)

nential tails. This is in itself a very interesting result, but a physical theory for $P_v(v)$ is not yet available. Note also that even for $n > 16$ the fluctuations of the velocity are not yet isotropic everywhere.

The skewness of the zonally averaged PDF, which is given by

$$S^z_\Phi = \frac{[\langle \Phi'^3 \rangle]}{[\langle \Phi'^2 \rangle]^{3/2}}, \tag{5}$$

generally does not coincide with $[S]$. The skewness S^z and $[S]$ are identical only if $P(\Phi') = [P(\Phi')]$. However, Fig. 5 shows that S^z and $[S]$ are qualitatively very similar with significant quantitative differences only at the lowest levels.

Finally, it is of interest to compare S_Φ from a GCM simulation with the observations. Here we had available 300-mb data from a 10-yr run (nine winters) of the Canadian Climate Centre (CCC) GCM (McFarlane et al. 1992), with a specified annual cycle of sea surface temperatures (i.e., no interannual variability in the forcing). The simulated and observed skewnesses are shown in Fig. 6 for DJF. The gross skewness patterns match quite well. The level of agreement is remarkable because at midlatitudes the actual moments, like the variance, are much too weak in the simulations. [This is a deficiency common to GCMs of that generation; see, e.g., Gates et al. (1990).] Inspection of the zonally averaged PDFs of the model data (not shown) suggests that the shape of the simulated PDF of Φ' is qualitatively similar to the one observed, with the GCM fluctuations being to a large degree scaled down versions of the observed fluctuations.

3. A diagnostic study of the skewness

We now proceed to dissect the balance equation to elucidate the mechanism that skews $P(\Phi')$. To this end we compute the terms on the rhs of the balance equation (1) using the nondivergent winds, in turn computed from the vorticity data. In this section we again consider fluctuations about a mean annual cycle that is approximated by a least-squares parabola as in the previous section. To demonstrate the validity and accuracy of the balance equation, we compare in Fig. 7 the variance and skewness of Φ, as explicitly obtained from the winds via the balance equation, to the observations.

Consider first the fluctuating contributions, Φ^c, to Φ that are due to the Coriolis force and represent the dominant linear term in the balance equation:

$$\nabla^2 \Phi^c = -\nabla \cdot (\mathbf{f} \times \mathbf{v}'). \tag{6}$$

If the statistics of $\mathbf{v}'$ were invariant under $\mathbf{v}' \to -\mathbf{v}'$, then Φ^c, being linear in $\mathbf{v}'$, would have zero skewness. The skewness of Φ^c as obtained from the observed winds is shown in Fig. 8. Clearly, the large-scale winds cannot be completely symmetric, as Φ^c has substantial skewness until the low wavenumbers have been discarded. Beyond wavenumber 8, Φ^c_8 has relatively little skewness, which contrasts sharply with the skewness of the complete Φ_8 field in Fig. 7, demonstrating that the nonlinear term of (1) is responsible for most of the skewness.

We now examine the contributions of various pieces of $\nabla\cdot(\mathbf{v}\cdot\nabla)\mathbf{v}$ to the skewness of Φ. Since we will be interested in Φ_{n_0} (Φ filtered by discarding wavenumbers less than n_0), a natural scale separation occurs at wavenumber $n_0/2$. Since the nonlinearity is quadratic, the interaction of two velocity modes both with wavenumbers less than $n_0/2$ cannot contribute to Φ_{n_0}. However, the interaction of two modes with $n < n_0$, but the sum of their wavenumbers exceeding n_0, can contribute to Φ_{n_0}. Not precisely every such interaction will contribute, but we are not interested in disentangling that level of detail. Here we simply separate $\mathbf{v}$ into a "large-scale" piece $\mathbf{v}^L$ and a "small-scale" piece $\mathbf{v}^S \equiv \mathbf{v} - \mathbf{v}^L$, where $\mathbf{v}^L$ denotes the velocity triangularly truncated at wavenumber $n_s \equiv n_0/2$ ($\mathbf{v}^L$ includes n_s). We can then explicitly remove $\mathbf{v}^L\mathbf{v}^L$ interactions from the balance equation and ask whether asymmetric large-scale velocity fluctuations make a contribution beyond n_0 via $\mathbf{v}^L\mathbf{v}^S$ interactions.

With this simple scale separation we write $(\partial_i v_j)(\partial_j v_i)$ as the sum of five terms as follows:

$$(\partial_i v_j)(\partial_j v_i) = \partial_i\partial_j[\underbrace{v_j'^S v_i'^S}_{\text{(term 1)}} + \underbrace{2\overline{v}_j v_i'^S}_{\text{(term 2)}} + \underbrace{2v_j'^L(\overline{v}_i^S + v_i'^S)}_{\text{(term 3)}} + \underbrace{(2\overline{v}_j^L v_i'^L + v_j'^L v_i'^L)}_{\text{(term 4)}} + \underbrace{\overline{v}_i\overline{v}_j}_{\text{(term 5)}}]. \quad (7)$$

By design, we can immediately discard term 4. Although term 5 is nonfluctuating, and hence does not formally contribute to the fluctuations of Φ, it is not entirely eliminated when removing a least squares parabolic seasonal trend from Φ. This is because $\overline{\mathbf{v}}$ is itself estimated as a parabola so that $\overline{v}_i\overline{v}_j$ is a quartic (in time, within a season). However, we explicitly checked that the cubic and quartic terms are negligible as expected (e.g., they contribute less than 0.1% to the skewness of Φ'), and therefore term 5 is safely neglected. The contribution of each of the remaining terms to Φ_{n_0} is obtained by applying the (negative) inverse Laplacian to it. We may therefore write the (filtered) fluctuations, $\Phi^B_{n_0}$, of the geopotential as determined by the balance equation as

$$\Phi^B_{n_0} = \Phi^c_{n_0} + \Phi^{(1)} + \Phi^{(2)} + \Phi^{(3)}, \quad (8)$$

with $\Phi^{(l)}$ corresponding to (term l) in (7). Thus $\Phi^{(1)}$ is the dominant nonlinear term in the fluctuations, $\Phi^{(2)}$

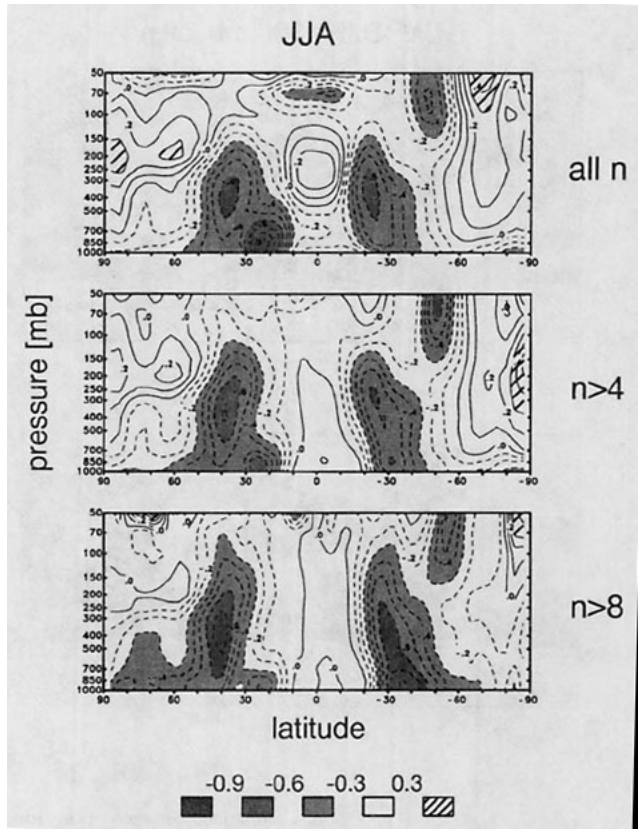

FIG. 5. The skewness of the zonally averaged PDFs of Φ' as a function of pressure and latitude. The contour spacing is 0.1.

TABLE 1. Variances and skewnesses corresponding to the PDFs of Fig. 4. (Variance units are 10^6 m^4 s^{-4} for Φ and m^2 s^{-2} for u and v).

		33.4°–26.0°N		3.71°N–3.71°S		37.1°–44.5°S	
		Variance	Skewness	Variance	Skewness	Variance	Skewness
Φ	all n	0.70 ± 0.03	−0.58 ± 0.02	0.04 ± 0.01	−0.10 ± 0.09	1.15 ± 0.06	−0.60 ± 0.01
	$n > 4$	0.65 ± 0.03	−0.70 ± 0.06	0.06 ± 0.01	0.00 ± 0.09	1.01 ± 0.04	−0.67 ± 0.05
	$n > 8$	0.30 ± 0.02	−0.71 ± 0.03	0.060 ± 0.009	0.02 ± 0.01	0.462 ± 0.004	−0.77 ± 0.07
	$n > 16$	0.037 ± 0.002	−0.22 ± 0.03	0.009 ± 0.003	−0.04 ± 0.04	0.049 ± 0.001	−0.34 ± 0.06
u	all n	153 ± 7	0.008 ± 0.007	30 ± 2	0.32 ± 0.08	130 ± 2	−0.017 ± 0.006
	$n > 4$	146 ± 6	0.0052 ± 0.0006	28 ± 3	0.203 ± 0.008	126 ± 2	−0.01 ± 0.02
	$n > 8$	88.0 ± 0.4	0.15 ± 0.02	23 ± 1	0.15 ± 0.01	91 ± 3	0.02 ± 0.04
	$n > 16$	25 ± 1	0.06 ± 0.02	8.1 ± 0.7	−0.014 ± 0.004	22 ± 1	0.03 ± 0.03
v	all n	120 ± 5	−0.03 ± 0.02	12 ± 1	0.025 ± 0.006	145.9 ± 0.5	0.048 ± 0.007
	$n > 4$	117 ± 5	−0.03 ± 0.03	12 ± 1	0.000 ± 0.008	143.6 ± 0.4	0.053 ± 0.004
	$n > 8$	66.8 ± 0.7	−0.15 ± 0.03	11 ± 1	0.01 ± 0.02	94 ± 4	0.081 ± 0.005
	$n > 16$	17.1 ± 0.9	−0.012 ± 0.001	4.3 ± 0.8	0.005 ± 0.002	21 ± 1	0.019 ± 0.005

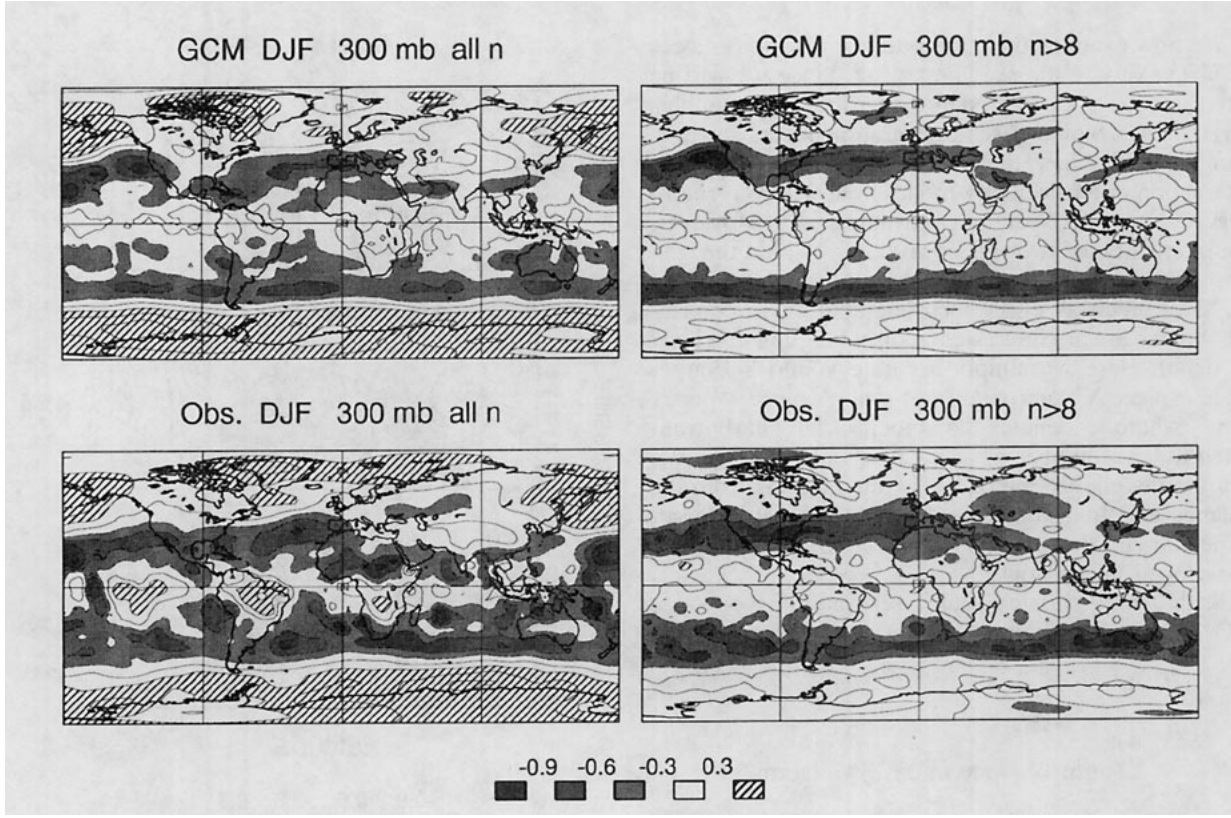

FIG. 6. Comparison between observations and CCC GCM data for the skewness of Φ at 300 mb, DJF. The contour interval is 0.3.

represents the interaction of the fluctuations with the mean state, and $\Phi^{(3)}$ represents the effect of large-scale fluctuations.

With a scale separation between wavenumbers 4 and 5 ($n_s = 4$), it turns out that the global spectra of $\Phi^{(1)}$ and $\Phi^{(2)}$ are of the same order of magnitude, while the spectrum of $\Phi^{(3)}$ is more than an order of magnitude smaller for $n > n_0 = 8$. We can therefore ignore $\mathbf{v}'^L$ altogether [we explicitly checked that neglecting $\Phi^{(3)}$ has no effect on the skewness of Φ_8]. The smallness of $\Phi^{(3)}$ is basically due to the fact that the large-scale velocities are primarily stationary. The spectrum of the fluctuating velocity, $E_{\mathbf{v}'}(n)$, is more than an order of magnitude smaller than the total spectrum, $E_{\mathbf{v}}(n)$, for $n \lesssim 5$. Beyond its peak at $n \sim 8$, $E_{\mathbf{v}} \sim E_{\mathbf{v}'}$. [For typical spectra of mean and transient velocities, see, e.g., Boer and Shepherd (1983).] If the scale separation is moved to higher wavenumber, $\mathbf{v}'^L$ becomes larger and $\Phi^{(3)}$ can no longer be neglected. For example, if the scale separation is at $n_s = 8$, $\Phi^{(1)}$, $\Phi^{(2)}$, and $\Phi^{(3)}$ are all of the same order.

Because the skewness is a highly nonlinear functional of Φ, the skewness is not usefully decomposed into additive contributions by expanding Φ as the sum (8) in expression (4) for S. To demonstrate the effect of $\Phi^{(1)}$ and $\Phi^{(2)}$ on the skewness of $\Phi^B_{n_0}$, we therefore compute the skewnesses of $\Phi^B_{n_0} - \Phi^{(1)}$ and $\Phi^B_{n_0} - \Phi^{(2)}$ and compare them with the skewnesses of $\Phi^B_{n_0}$ and $\Phi^c_{n_0}$ in Fig. 9a for $n_0 = 8$ ($n_s = 4$) and in Fig. 9b for $n_0 = 0$ (no filtering, no scale separation). The figure shows both seasons at 400 mb where the skewness is approximately maximized and at 200 mb, the approximate level of the climatological jets, where the velocity variance is approximately maximized. Figure 9 clearly shows that $\Phi^{(1)}$ is responsible for the large negative skewness bands for both the full and filtered Φ.

The effect of $\Phi^{(2)}$ (interaction with the mean state) is small but clearly observable at 200 mb, where both the mean gradient and the fluctuations are near their maxima. For the filtered data ($n_0 = 8$), the asymmetries in Φ^c are small and the effect of $\Phi^{(2)}$ is particularly clean: $\Phi^{(2)}$ tends to reduce the skewness in the strong-flow winter hemisphere. In fact, if it were not for $\Phi^{(2)}$, the skewness would be maximized in the winter hemisphere. This makes some intuitive sense since $\Phi^{(2)}$, being linear in the fluctuations, adds to the Coriolis term, making the nonlinearities relatively less important. Roughly, $\Phi^{(2)}$ contributes more to the denominator than to the third moment, although this statement is generally only true for asymptotically large $\Phi^{(2)}$. For small and $O(1)$ values of the mean vorticity and strain (nondimensionalized by f), the presence of $\Phi^{(2)}$ can actually enhance the skewness (see section 4). In the winter hemisphere, at this level, a stronger $\Phi^{(2)}$ hap-

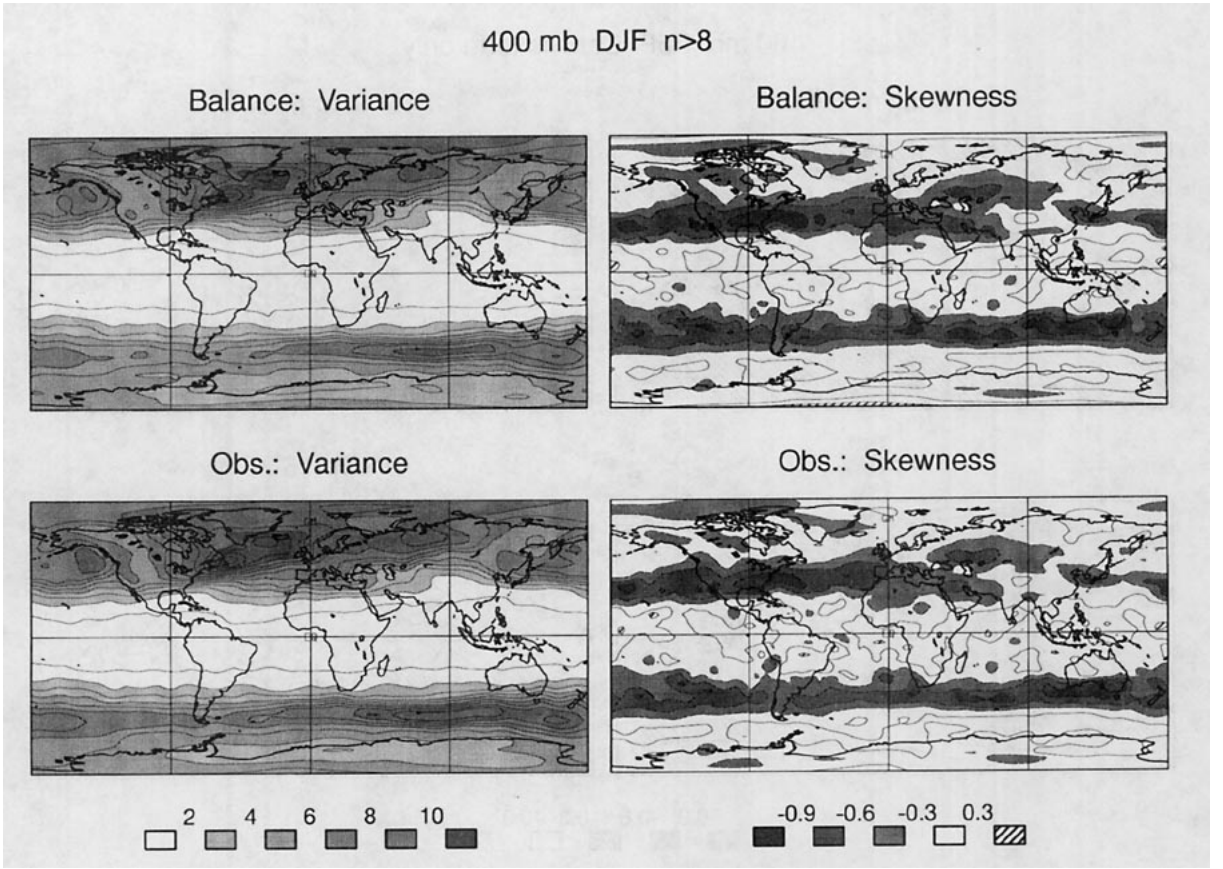

FIG. 7. Comparison of the variance and skewness of Φ as obtained from the balance equation with observations. The contour spacing for the variance is 10^5 m^4 s^{-4}, and for the skewness 0.3.

pens to compensate for a stronger $\Phi^{(1)}$, giving Φ a skewness not much different from that in the summer hemisphere.

Below the level of the jets, the effect of $\Phi^{(2)}$ on modulating the midlatitude skewness is small, but the negative skewness of Φ^c is largest there and larger in the summer than in the winter hemisphere (Figs. 8 and 9). We therefore attribute the fact that the negative skewness is maximized below the level of the jets and generally in the summer hemisphere to the presence of asymmetries in the velocity itself. This assertion has further support from the analytic considerations of the next section, where we find that for Gaussian velocities the extrema of $[S]$ do correspond to the maxima of the zonally averaged velocity variance.

Finally, it is interesting to look at the skewness of $\Phi^{(1)}$ in isolation. For idealized Gaussian, homogeneous, isotropic velocity fluctuations, $\Phi^{(1)}$ has a skewness that is negative definite and a function of the form of the spectrum only, independent of the eddy kinetic energy (see HS and below). Thus, departures of $S_{\Phi^{(1)}}$ from a constant value are indications to what degree the skewness is sensitive to the velocity being non-Gaussian, inhomogeneous, and anisotropic. Figure 10 shows $[S_{\Phi^{(1)}}]$ for $n_s = 4$ and 8 for both $\Phi^{(1)}$ unfiltered and filtered by removing wavenumbers $n < 2n_s$. The unfiltered $\Phi^{(1)}$ has very large negative skewness with a dip in the Tropics, where the skewness drops by a factor of ~ 2. Nevertheless, the skewness of $\Phi^{(1)}$ is much more slowly varying than the skewness of Φ and could be argued to be roughly constant from $\sim 15°$ to $\sim 80°$ in both hemispheres. Filtering $\Phi^{(1)}$ drastically reduces the skewness and imposes additional structure.

4. Analytical arguments and models for the PDF of Φ

To gain some insight into how key flow parameters control the skewness and functional form of $P(\Phi')$, we consider here idealized fluctuations that are analytically tractable on a beta plane. We assume that all mean quantities, such as kinetic energy, spectra, and mean velocity gradients are constant throughout the beta plane with values determined at the origin. [For simplicity, we ignore in this section the presence of a seasonal trend within a season, so that $\bar{X} = \langle X \rangle$, for any variable X.] Superposed on this (locally) constant mean background flow, fluctuating velocities are assumed to be homogeneous, isotropic, and Gaussian. While this is clearly not the case in the atmosphere on

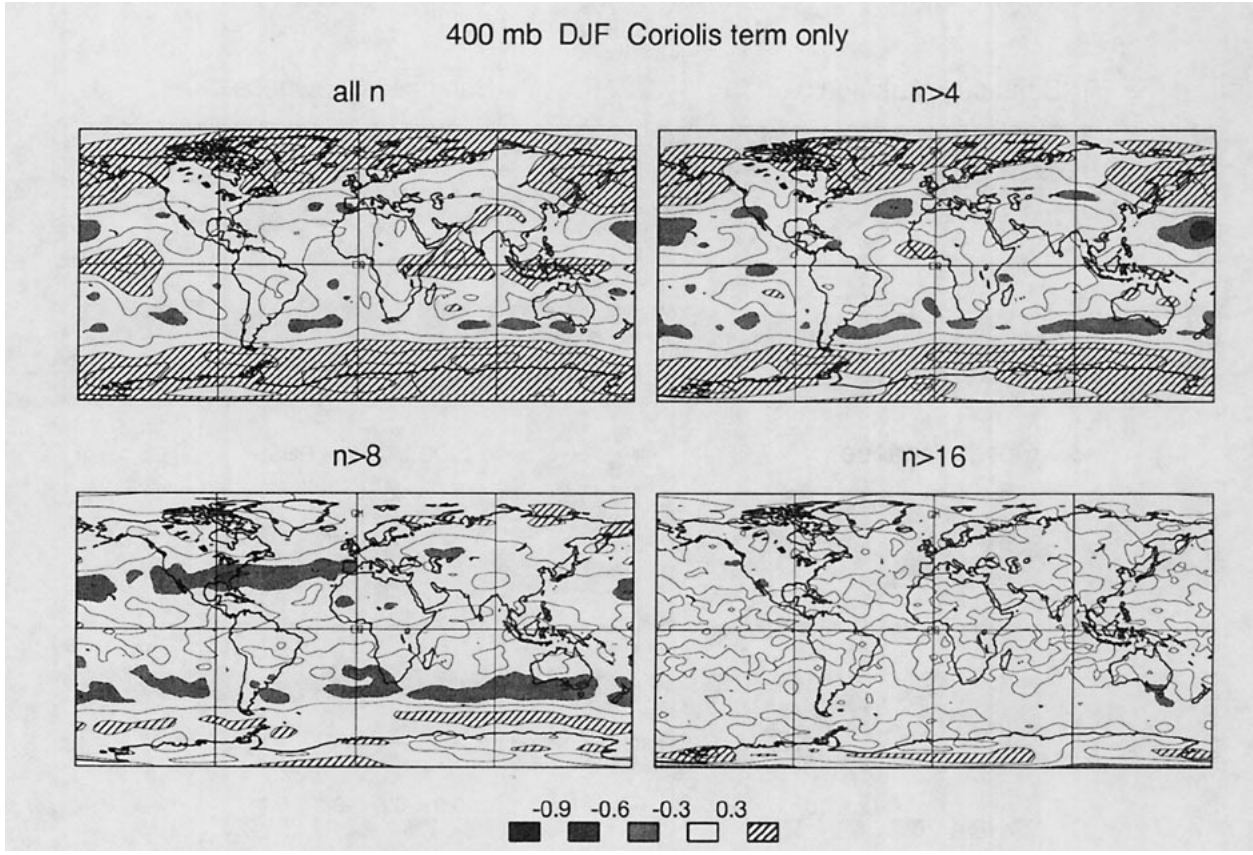

FIG. 8. The skewness of the Coriolis contribution, Φ^c, to Φ at 400 mb, DJF. The contour interval is 0.3.

all scales, there is some evidence that homogeneity and isotropy are reached at sufficiently high wavenumber ($n \geq 10$) (Boer 1994). As was shown in the previous section, the very large scales can essentially be ignored when one is interested in the fluctuations of Φ_8. The idea here is to learn what one can by simply assuming that the flow on all relevant scales is multivariate Gaussian, homogeneous, and isotropic and that interactions with inhomogeneous, anisotropic, non-Gaussian fluctuations can be ignored. Interactions with the mean flow are not necessarily negligible, and we will therefore keep the $\partial_i \bar{v}_j \partial_j v_i$ term. Inhomogeneities in the fluctuations of Φ will be captured by moving the beta plane from place to place. Figure 4 showed that at least the one-point PDF of u is close to Gaussian when the large scales have been discarded, but that the v component, while symmetric, can deviate from being Gaussian. Without being very far from observations, we will take the flow to be precisely multipoint Gaussian as this is the only case for which formally infinite-dimensional multivariate statistics are analytically tractable. In the concluding remarks following this section, we will revisit the assumption of a multivariate Gaussian flow and discuss its physical limitations.

With these preliminary considerations we write the balance equation on the beta plane ($f = f_0 + \beta y$) as

$$\nabla^2 \Phi = -(\partial_i v_j)(\partial_j v_i) - 2\partial_i \bar{v}_j \partial_j v_i - \beta u + f_0 \zeta + (\text{nonfluctuating}), \quad (9)$$

where we have dropped the primes on the rhs so that all unbarred velocities denote the zero-mean fluctuations. With the assumptions made, Φ as given by (9) has manifestly homogeneous statistics.

Expressing the velocity in terms of the streamfunction, $(u, v) = (-\partial_y, \partial_x)\psi$, and inverting the Laplacian in (9), we find that the geopotential at the origin [$\mathbf{x} = (x, y) = \mathbf{0}$] is given by

$$\Phi(\mathbf{0}) = -\int (d\mathbf{q}_1)(d\mathbf{q}_2)\tilde{\psi}(\mathbf{q}_1)\left(\frac{\mathbf{q}_1 \times \mathbf{q}_2}{\mathbf{q}_1 - \mathbf{q}_2}\right)^2 \tilde{\psi}^*(\mathbf{q}_2) + \int (d\mathbf{q})\tilde{\psi}(\mathbf{q})[f_0 - \bar{\zeta} - \Sigma(\mathbf{q}) + i\beta q_y/q^2], \quad (10)$$

where $(d\mathbf{q})$ denotes $dq_x dq_y/(2\pi)^2$, $\tilde{\psi}(\mathbf{q}) = \int d\mathbf{x}\psi(\mathbf{x}) \times \exp(-i\mathbf{q}\cdot\mathbf{x})$, and

$$\Sigma(\mathbf{q}) \equiv 2[2\bar{s}_{xx} q_x q_y + \bar{s}_{xy}(q_y^2 - q_x^2)]/q^2, \quad (11)$$

with $\bar{s}_{ij} \equiv (\partial_i \bar{v}_j + \partial_j \bar{v}_i)/2$ being the mean strain field. Here $\Phi(\mathbf{0})$ is the full Φ field at the origin. Filtering Φ analytically would add a great deal of complexity to

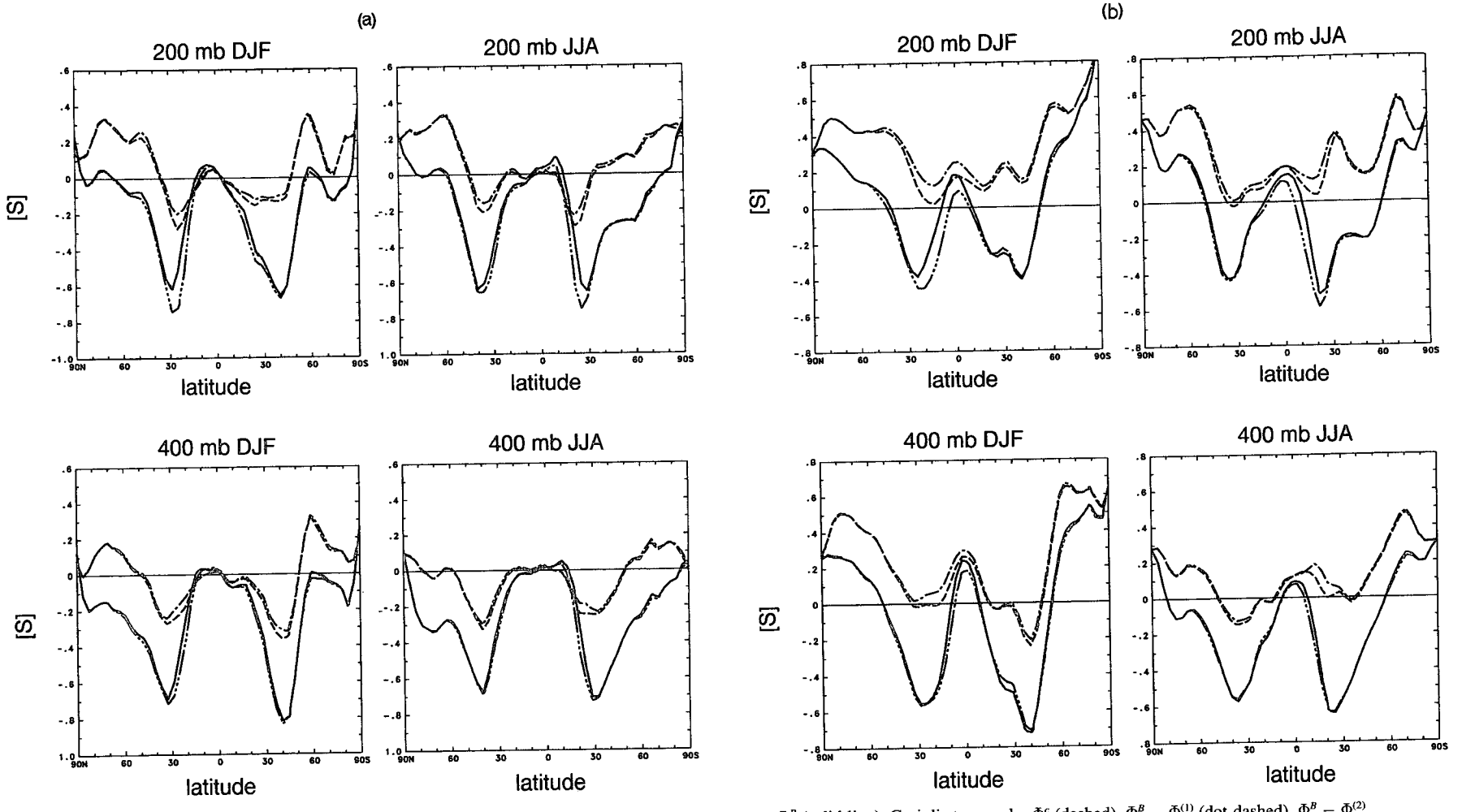

FIG. 9. Zonally averaged skewness of various terms in the balance equation: sum of all terms, Φ^B (solid line), Coriolis term only, Φ^c (dashed), $\Phi^B - \Phi^{(1)}$ (dot-dashed), $\Phi^B - \Phi^{(2)}$ (triple-dot-dashed). (a) Only wavenumbers $n > 8$ are retained, with a scale separation between wavenumbers 4 and 5. (b) Skewness of the unfiltered fields without any scale separation.

the subsequent analysis and unnecessarily obscure what simple results can be obtained.

It is convenient to work not directly with $P(\Phi)$ but with its generating function $\tilde{P}(z) \equiv \int d\Phi P(\Phi) \times \exp(iz\Phi)$, which is given by

$$\tilde{P}(z) = \langle e^{iz\Phi(\mathbf{0},[\psi])} \rangle, \tag{12}$$

where the brackets $\langle\ \rangle$ denote an average over an ensemble of all possible fields ψ, and the notation $\Phi(\mathbf{0}, [\psi])$ emphasizes the functional dependence of Φ on ψ. From the generating function, moments of the distribution are easily evaluated via

$$\langle \Phi^n \rangle = (-i)^n \left(\frac{\partial^n}{\partial z^n} \tilde{P}(z) \right)_{z=0}. \tag{13}$$

Note that $P(\Phi)$ is normalized when $\tilde{P}(z = 0) = 1$ and that the asymptotic properties of $P(\Phi)$ are determined by the analytic structure of $\tilde{P}(z)$ in the complex z-plane.

Because $\mathbf{v}$ is homogeneous and isotropic,

$$\langle \tilde{\psi}(\mathbf{p})\tilde{\psi}(\mathbf{q}) \rangle = (2\pi)^2 \delta(\mathbf{p} + \mathbf{q}) \sigma^2(q), \tag{14}$$

where $\sigma(q)$ is related to the kinetic energy spectrum, $E(q)$, normalized so that $\int dk E(k) = \langle |\mathbf{v}|^2 \rangle / 2$, via $\sigma^2(q) = 4\pi E(q)/q^3$. Because we assumed that the fluctuations are Gaussian, all the Fourier modes are independent via (14), except where related through $\psi(\mathbf{q}) = \psi^*(-\mathbf{q})$ by virtue of reality. Thus, the ensemble average of (12) becomes

$$\tilde{P}(z) = \mathcal{N} \int \left(\prod_{\mathbf{q}} d\tilde{\psi}(\mathbf{q}) \right) \exp\left\{ -\int (d\mathbf{q}) \frac{\tilde{\psi}^*(\mathbf{q})\tilde{\psi}(\mathbf{q})}{2\sigma(q)^2} \right\}$$

$$\times \exp\{ iz\Phi(\mathbf{0}, [\psi]) \} = \mathcal{N} \int (\mathcal{D}\tilde{\psi})$$

$$\times \exp\left\{ -\int (d\mathbf{p})(d\mathbf{q}) \chi(\mathbf{q}) B(\mathbf{q}, \mathbf{p}) \chi^*(\mathbf{p}) \right.$$

$$\left. - iz \int (d\mathbf{p}) F(\mathbf{p}) \chi(\mathbf{p}) \right\}, \tag{15}$$

where the product (i.e., the functional integral) is over only one-half of the $\mathbf{q}$ because $\psi(\mathbf{q}) = \psi^*(-\mathbf{q})$, $\mathcal{N}$ is a normalizing constant, $\chi(\mathbf{q}) \equiv \tilde{\psi}(\mathbf{q})/(\sqrt{2}\sigma(q))$ is the scaled streamfunction,

$$B(z; \mathbf{p}, \mathbf{q}) \equiv (2\pi)^2 \delta(\mathbf{p} - \mathbf{q}) + izM(\mathbf{p}, \mathbf{q}), \tag{16}$$

and

$$F(\mathbf{q}) \equiv \sqrt{2}\sigma(q)[f_0 - \bar{\zeta} - \Sigma(\mathbf{q}) + i\beta q_y/q^2], \tag{17}$$

with

$$M(\mathbf{p}, \mathbf{q}) \equiv 2\sigma(p) \left(\frac{\mathbf{p} \times \mathbf{q}}{\mathbf{p} - \mathbf{q}} \right)^2 \sigma(q). \tag{18}$$

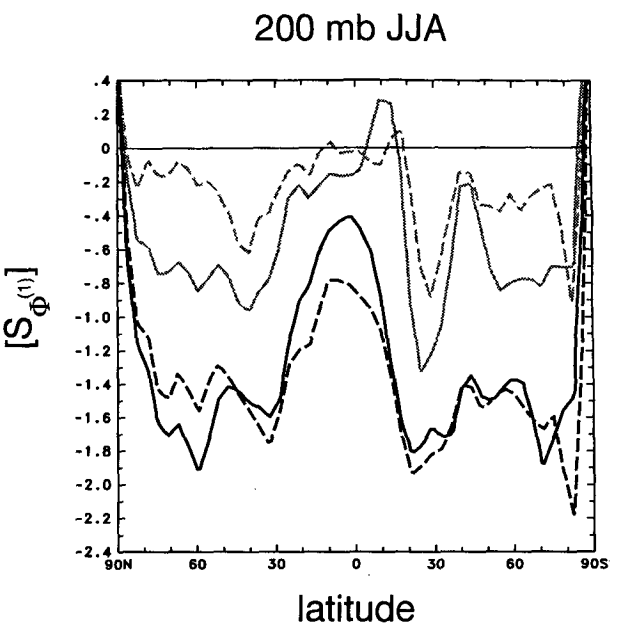

FIG. 10. Skewness of the nonlinear term $\Phi^{(1)}$ in isolation. The solid line is for scale separation at wavenumber $n_s = n_0/2 = 4$, the dashed line for scale separation at $n_s = n_0/2 = 8$. The gray lines correspond to the skewness of $\Phi^{(1)}$ filtered by discarding wavenumbers $n \leq n_0$, while the black lines are the corresponding skewnesses of the unfiltered field.

We may think of B and M as matrices $\mathbf{B}$, $\mathbf{M}$, with continuous indices $\mathbf{p}$ and $\mathbf{q}$ (or discrete indices for a finite-dimensional discretized version of the equations). Similarly, we may think of $F(\mathbf{p})$ as a vector $\mathbf{F}$. To keep notation maximally simple, we adopt this matrix notation with the inner product defined as the integral over repeated continuous indices with, for example, measure $\int (d\mathbf{p})$ for index $\mathbf{p}$, in direct analogy with the discrete case. Thus, for example, the trace of $\mathbf{M}^2$, denoted by $\mathrm{Tr}(\mathbf{M}^2)$, stands for $\int (d\mathbf{p})(d\mathbf{q}) M(\mathbf{p}, \mathbf{q}) M(\mathbf{q}, \mathbf{p})$, and $\det(\mathbf{M})$ stands for the determinant of $\mathbf{M}$, which is equivalent to $\exp\{\mathrm{Tr}[\log(\mathbf{M})]\}$. The transpose of $\mathbf{F}^*$ is denoted by $\mathbf{F}^\dagger$. Since the exponent in (15) is a quadratic functional, $\tilde{P}(z)$ is readily evaluated via standard methods as

$$\tilde{P}(z) = \frac{1}{\sqrt{\mathrm{Det}(\mathbf{B}(z))}} \exp\left[-\frac{z^2}{4} \mathbf{F}^\dagger \cdot \mathbf{B}^{-1}(z) \cdot \mathbf{F} \right], \tag{19}$$

where $B^{-1}(\mathbf{p}, \mathbf{q})$ is defined through $\int (d\mathbf{q}') B^{-1}(\mathbf{p}, \mathbf{q}') B(\mathbf{q}', \mathbf{q}) = (2\pi)^2 \delta(\mathbf{p} - \mathbf{q})$, that is, $\mathbf{B}^{-1} \cdot \mathbf{B} = \mathbf{1}$.

Equation (19) shows that the generating function has singularities where $\det(\mathbf{B}(z)) = 0$. The terms in the exponent do not introduce any further singularities since $\mathbf{B}^{-1}(z)$ is singular only where $\det(\mathbf{B}(z)) = 0$. The zeros of $\det(\mathbf{B})$ occur for purely imaginary z by virtue of $\mathbf{M}$ being real and symmetric (HS). The zero closest to the real axis occurs at $z = i/\lambda$, where λ is the largest (in absolute value) eigenvalue of $\mathbf{M}$. It follows

from standard theorems on Fourier transforms that for large $|\Phi|$ the PDF, $P(\Phi)$, has an exponential tail of the form $P(\Phi) \sim \exp(-|\Phi/\lambda|)$. The magnitude of the largest eigenvalue, λ, is bounded by its estimate of $2\langle|\mathbf{v}(\mathbf{0})|^2\rangle$ (the matrix $\mathbf{M}$ differs by a factor of 2 from that defined in HS). For small values of Φ, the singularities of $\tilde{P}(z)$ can be ignored, so that we may take $\mathbf{B} \sim \mathbf{B}^{-1} \sim 1$. The resulting integral is trivial and shows that for small Φ, $P(\Phi)$ is approximately Gaussian, that is, $P(\Phi) \sim \exp(-\Phi^2/\mathbf{F}^\dagger\cdot\mathbf{F})$. The crossover from this central Gaussian core to the ultimate exponential tails thus occurs at $\Phi \sim \Phi_e \equiv \mathbf{F}^\dagger\cdot\mathbf{F}/\langle|\mathbf{v}(\mathbf{0})|^2\rangle$.

Whether or not one actually can see the exponential tail of $P(\Phi)$ depends on how many standard deviations Φ_e represents. The variance of Φ can be computed from (19) and (13) as

$$\langle\Phi'^2\rangle = \frac{1}{2}(\mathrm{Tr}(\mathbf{M}^2) + \mathbf{F}^\dagger\cdot\mathbf{F}), \tag{20}$$

where $\Phi' \equiv \Phi - \langle\Phi\rangle$. The first term in (20) can be bounded by its estimate of $4\langle|\mathbf{v}(\mathbf{0})|^2\rangle^2$ so that

$$\Phi_e/\sigma_\Phi \sim \frac{2\sqrt{2}}{R}\frac{1}{\sqrt{1+R^2}}, \tag{21}$$

where

$$R \equiv \frac{2\langle|\mathbf{v}(\mathbf{0})|^2\rangle}{\sqrt{\mathbf{F}^\dagger\cdot\mathbf{F}}}, \tag{22}$$

and $\sigma_\Phi \equiv \sqrt{\langle\Phi'^2\rangle}$. The bounds of the integrals in (20) are simply accomplished by realizing that $M(\mathbf{p}, \mathbf{q}) \leq 2\sigma(p)\sigma(q)pq$, which allows factorization of the integrals. For the special case of no mean vorticity or strain, $F(\mathbf{q}) = \sqrt{2}\sigma(q)(f_0 + i\beta q_y/q^2)$, so that $\mathbf{F}^\dagger\cdot\mathbf{F} = 4\int dqE(q)(f_0^2 + \beta^2 q_y^2/q^4)/q^2$. Thus, if we define length scales, L, L_y, and a velocity scale, V, through $V^2L^2(f_0^2 + \beta^2L_y^2) = \int dqE(q)(f_0^2 + \beta^2q_y^2/q^4)/q^2$ and $V^2 \equiv \langle|\mathbf{v}(\mathbf{0})|^2\rangle$, R is recognized as the Rossby number, $V/(f_0L)$, appropriate for scale L when $\beta = 0$, and as a generalized nonsingular Rossby number, $V/(L\sqrt{f_0^2 + \beta^2L_y^2})$, for nonzero β (and similarly for nonzero $\partial_i\bar{v}_j$). When the balance is dominated by the linear terms (small kinetic energy, large $\mathbf{F}$), R is small and the tail occurs for an unobservably large number ($\propto 1/R$) of standard deviations.

Explicit expressions for higher moments of Φ can be computed again via (19) and (13) or directly by taking moments of (10). Since ψ is assumed to be Gaussian, averages of an odd number of ψs vanish and averages of $2n$ products of ψ decompose into products of n averages of the form $\langle\psi\psi\rangle$ as given by (14), paired in all possible ways. Either way, one obtains for the third and fourth moments

$$\langle\Phi'^3\rangle = -\mathrm{Tr}(\mathbf{M}^3) - \frac{3}{2}\mathbf{F}^\dagger\cdot\mathbf{M}\cdot\mathbf{F}, \tag{23}$$

and

$$\langle\Phi'^4\rangle = 3\,\mathrm{Tr}(\mathbf{M}^4) + 6\mathbf{F}^\dagger\cdot\mathbf{M}^2\cdot\mathbf{F} + \frac{3}{4}[\mathrm{Tr}(\mathbf{M}^2) + \mathbf{F}^\dagger\cdot\mathbf{F}]^2. \tag{24}$$

From (20) and (23), the skewness is given by $S = \langle\Phi'^3\rangle/\langle\Phi'^2\rangle^{3/2}$. To determine the generic dependence of the skewness on the generalized Rossby number (22), we again estimate the integrals of (23) by their bounds. The term $\mathbf{F}^\dagger\cdot\mathbf{M}\cdot\mathbf{F}$ is not positive definite for arbitrary $\Sigma(\mathbf{q})$ [defined in (11)], so that we will only estimate its magnitude. Again bounding $M(\mathbf{p}, \mathbf{q}) \leq 2\sigma(p)\sigma(q)pq$, we have $\mathrm{Tr}(\mathbf{M}^3) \sim 8\langle|\mathbf{v}(\mathbf{0})|^2\rangle^3$, and replacing $\mathbf{F}$ by $|\mathbf{F}|$, $|\mathbf{F}^\dagger\cdot\mathbf{M}\cdot\mathbf{F}| \leq 2(\int(d\mathbf{p})|\mathbb{F}(\mathbf{p})|\sigma(p)p)^2 \leq 2\mathbf{F}^\dagger\cdot\mathbf{F}\langle|\mathbf{v}(\mathbf{0})|^2\rangle$, where the last inequality follows as a Cauchy–Schwartz inequality. Thus, we obtain

$$S \sim -2\sqrt{2}R\frac{(\text{const.}) + R^2}{(1+R^2)^{3/2}}, \tag{25}$$

where (const.) is $O(1)$ with a sign that depends on the details of $\Sigma(\mathbf{q})$. For small R, $S \propto \pm R$, while for large R, S approaches a negative constant.

Equations (23) and (20) cannot be evaluated in closed form for a power-law spectrum, so that it is illuminating to consider a δ-function spectrum positioned at wavenumber n_δ. We will refer to this model as the "shell model" since the streamfunction lives on a (circular) shell in spectral space. For this special case even the generating function itself can be obtained in closed form. Although this can in principle be accomplished by direct substitution into (19), it is much simpler to start with the expression (10) for $\Phi(\mathbf{0})$, restrict the wavevectors to lie on a circle, and then diagonalize by expanding the Fourier modes of $\tilde{\psi}(\mathbf{q})$ in circular harmonics. The Gaussian integrals over the amplitudes of those harmonics can then easily be performed. (For details on the technique, see the appendix of HS.) One obtains for the generating function $\tilde{P}(Z)$ of the PDF, $P(2\Phi/\langle|\mathbf{v}|^2\rangle)$,

$$\tilde{P}(Z) = \frac{1}{(1+iZ)\sqrt{1+2iZ}}\exp\left[-\frac{Z^2}{4\pi^2\,\mathrm{Ro}^2}\times\left(2\frac{(1-\hat{\bar{\zeta}})^2}{1+2iZ} + \frac{\hat{\beta}^2}{1+iZ} + 4(\hat{\bar{s}}_{xx}^2 + \hat{\bar{s}}_{xy}^2)\right)\right], \tag{26}$$

where $\mathrm{Ro} \equiv \sqrt{\langle|\mathbf{v}|^2\rangle}/(f_0L)$ is the (standard) Rossby number, $L \equiv 2\pi a/n_\delta$, $\hat{\bar{\zeta}} \equiv \bar{\zeta}/f_0$, $\hat{\bar{s}}_{ij} \equiv \bar{s}_{ij}/f_0$, and $\hat{\beta} \equiv \beta a/(n_\delta f_0) = (\cot\phi)/n_\delta$, with a being the earth's radius. From this generating function, we obtain the skewness

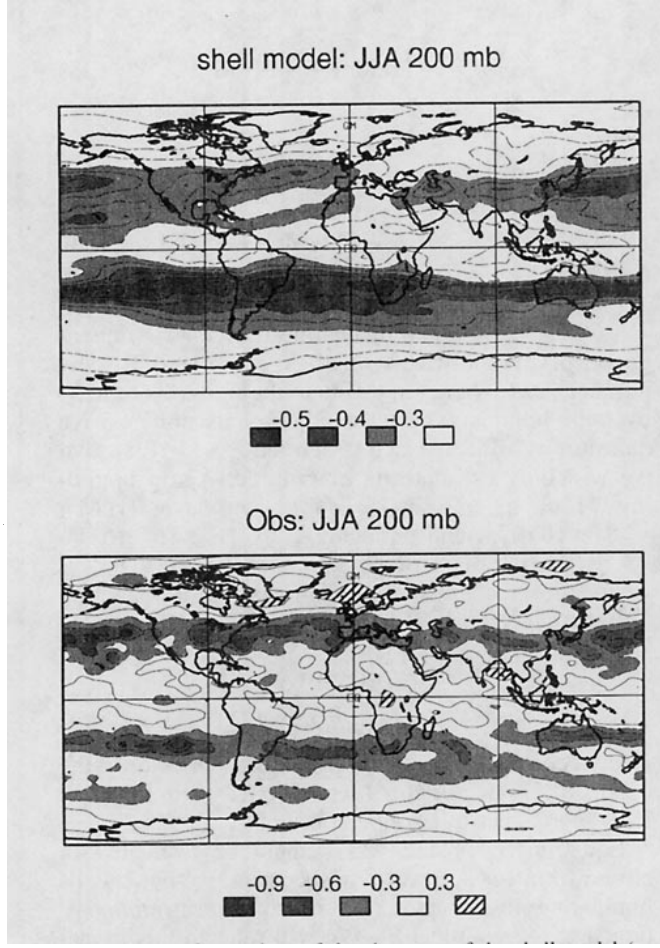

FIG. 11. (a) Comparison of the skewness of the shell model ($n_\delta = 4$) with the skewness of Φ_8 from the observations at 200 mb, JJA. The contour spacing is 0.05 for the shell model and 0.3 for the observations.

$$S_\delta = -\sqrt{2}\pi\,\mathrm{Ro}\,\frac{12(1-\hat{\bar{\zeta}})^2 + 3\hat{\beta}^2 + 20\pi^2\,\mathrm{Ro}^2}{(2(1-\hat{\bar{\zeta}})^2 + 4(\hat{\bar{s}}_{xx}^2 + \hat{\bar{s}}_{xy}^2) + \hat{\beta}^2 + 6\pi^2\,\mathrm{Ro}^2)^{3/2}}. \quad (27)$$

Note that S_δ has the general dependence on Ro given by (25) but is negative definite. Equation (27) can also be expressed in terms of the generalized Rossby number (22), which is given by $R = 4\pi\,\mathrm{Ro}(2(1-\hat{\bar{\zeta}})^2 + 4(\hat{\bar{s}}_{xx}^2 + \hat{\bar{s}}_{xy}^2) + \hat{\beta}^2)^{-1/2}$. In the limit of infinite Ro (with everything else constant), $S_\delta \to -10/(3\sqrt{3}) \sim -1.92\ldots$, which compares well with the unfiltered curves of Fig. 10, which show $[S_{\Phi^{(1)}}] \sim -1.6 \pm 0.3$ over a relatively wide range of latitudes.

It is interesting to evaluate S_δ at every point in the atmosphere with the local values of Ro, f_0, β, $\bar{\zeta}$, and $\bar{s}_{ij}$. The shell model has one major adjustable parameter, the radius of the shell, n_δ. The spectrum of the nonlinear contribution to Φ is easily shown to be $\propto n[1 - (n/(2n_\delta))^2]^2$ for $n \leqslant 2n_\delta$, and for $n > 2n_\delta$ the spectrum must of course vanish. Thus, to compare S_δ with the observed skewness of Φ_8, one should take $n_\delta \sim 4$–8. We find that with $n_\delta = 4$, we actually get some qualitative agreement with the observations (Fig. 11), although with such small n_δ the original picture of a beta plane throughout which the mean state is constant is somewhat stretched. The magnitude of $|S_\delta|$ is too small, but the pattern of its geographic variation is remarkably similar to the observations, considering the crudeness of the shell model.

Figure 12a shows $[S_\delta]$. Unlike in the observations (Fig. 2a), $|[S_\delta]|$ is largest where the zonally averaged velocity variance is strongest. In Fig. 12b the effect of the interaction with the mean state is illustrated by removing this term [setting $\bar{\zeta} = \bar{s} = 0$ in (27)]. In the atmosphere $\bar{s}_{xx}$ is small compared to $\bar{s}_{xy} \sim \bar{\zeta}/2$, ($\partial_x v \ll \partial_y u$), so that we can simply concentrate on the effect of the mean vorticity. The larger $\bar{\zeta}$, the larger the net linear contribution to Φ, and hence one would expect the presence of a large $\bar{\zeta}$ on either side of the jet to reduce $|S|$ and thus narrow the latitudinal extend of significant S, as indeed seen in Fig. 12a. However, $|S_\delta|$ is not a monotonically decreasing function of $\bar{\zeta}$ for fixed Ro and $\hat{\beta}$. For midlatitude values of Ro and $\hat{\beta}$, $|S_\delta|$ can in fact increase with an increase in $\bar{\zeta}$, for small

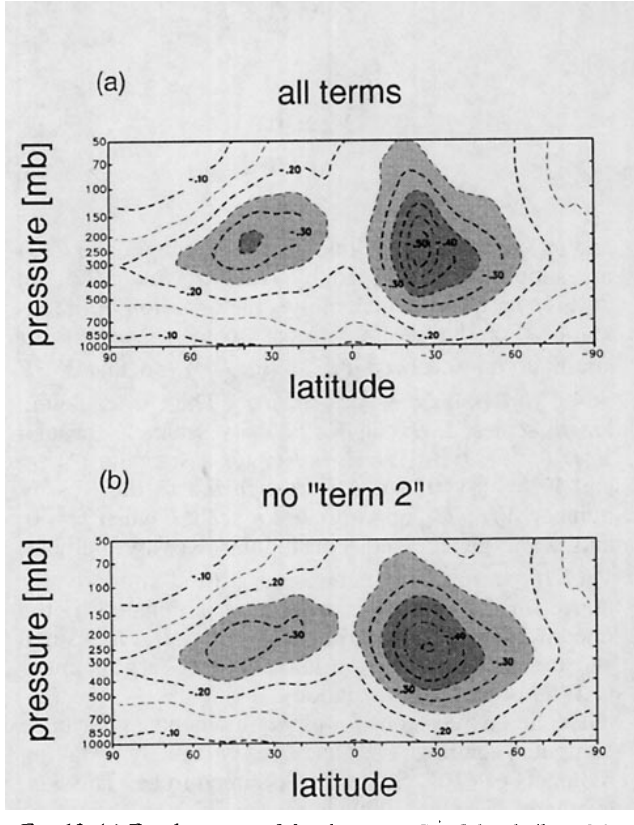

FIG. 12. (a) Zonal average of the skewness, S_δ, of the shell model ($n_\delta = 4$) for JJA. (b) As in (a) but with $\bar{\zeta} = 0$ and $\bar{s} = 0$, which corresponds to the skewness of $\Phi - \Phi^{(2)}$. The contour interval is 0.05, with light shading for $-0.35 < S_\delta \leqslant -0.25$ and dark shading for $S_\delta \leqslant -0.35$.

$|\hat{\zeta}|$ and $\hat{\zeta} \sim 1$! This is responsible for the higher maximum when $\hat{\zeta}$ is included (Fig. 12a). This example stresses that the dependence of the skewness on flow parameters can be quite subtle and that it is generally only asymptotically true that increasing the amplitude of the linear terms will decrease the skewness by increasing the denominator faster than the third moment.

5. Concluding remarks

The main point of this paper is to demonstrate that the dominant mechanism responsible for the large negative skewness of Φ is the rectification of near-symmetric velocity fluctuations by the advective nonlinearity. We have shown that this mechanism accounts for most of the observed negative skewness by computing the linear and nonlinear terms of the balance equation separately from the observed nondivergent winds. Because the linear terms have much less skewness when spatially filtered, the effect of the nonlinear term on Φ_8 is particularly clean. For Φ_8, interactions with asymmetric fluctuations with wavenumbers $n < 5$ could be neglected. Interactions with the mean flow have an observable effect on the skewness in the vicinity of the climatological jets, where both fluctuations and mean gradients are largest. At 200 mb the interactions with the mean flow are responsible for suppressing a winter hemisphere negative skewness maximum for Φ_8, although their effect is not large enough to explain the observed summer hemisphere negative skewness maximum at other levels and for the unfiltered data.

To obtain analytical results for $P(\Phi)$ and its skewness, we consider multivariate Gaussian, homogeneous, isotropic fluctuations on a beta plane. For such fluctuations, we show that $P(\Phi)$ has asymptotically exponential tails. The number of standard deviations that fluctuations must exceed to fall in the exponential regime scales with the strength of the nonlinear terms as measured by the generalized Rossby number, R, like $1/R$ [cf. (21) and (22)]. Consistent with these conclusions, in Fig. 4, approximate exponential tails are visible at midlatitudes, while in the Tropics $P(\Phi)$ is close to Gaussian. Confining Fourier modes to a shell in wavenumber allows closed-form expressions for the PDF and skewness, which show that the dependencies on the flow parameters can be quite subtle: increasing linear terms can actually increase the skewness. While the shell model does capture the gross geographic distribution of the skewness, maxima of the zonally averaged negative skewness coincide approximately with the maxima of the zonally averaged (transient) eddy kinetic energy, with the largest skewness occurring in the winter hemisphere. Although a Gaussian model with a full kinetic energy spectrum whose form is allowed to change from place to place could in principle produce a skewness pattern that is maximized ~150 mb below the velocity variance maxima and in the summer hemisphere, it is hard to imagine small inhomogeneities in the *form* of the spectrum to have a significant effect on the skewness pattern since inhomogeneities in the eddy kinetic energy are already taken into account in the shell model.

The most important shortcoming of a Gaussian model for the velocity is that it ignores asymmetries in the flow itself that are not negligible in the atmosphere, as could be seen from the skewness of the dominant linear contribution, Φ^c, to Φ (Fig. 8). These asymmetries affect the statistics of both the linear and nonlinear terms of the balance equation. Since the negative skewness of Φ^c is largest below the velocity maxima and in the summer hemisphere (Figs. 8 and 9), we attribute the fact that negative skewness maxima lie below the zonally averaged jets and are generally larger in the summer hemisphere to non-Gaussian behavior of the velocity field.

The asymmetries of the velocity have of course physical content. The nonvanishing of triple correlations, $\langle v_i'(\mathbf{x}_1)v_j'(\mathbf{x}_2)v_k'(\mathbf{x}_3)\rangle$ (for positions $\mathbf{x}_1$, $\mathbf{x}_2$, $\mathbf{x}_3$), simply expresses the fact that in turbulent flow there must be nonlinear transfer of kinetic energy and enstrophy across scales and, for an inhomogeneous system, net transport across space. Such correlations have been studied for homogeneous, isotropic turbulence and in the atmosphere for globally averaged energy and estrophy budgets, but little seems to be known about their spatial structure in the atmosphere. Of course, even for three-dimensional isotropic turbulence, where the triple correlations are known exactly through the von Kármán–Howarth relation (von Kármán and Howarth 1938; see also Landau and Lifshitz 1987, pp. 135–142.), it has not yet been possible to incorporate these correlations into an analytically tractable multivariate probability ensemble.

The nonvanishing of the triple correlations already contributes to the skewness of Φ^c. Consider for simplicity the beta-plane case of (9), for which we have

$$\langle \Phi^c(\mathbf{0})^3\rangle = f_0^3\langle \psi(\mathbf{0})^3\rangle + \int (d\mathbf{q}_1)(d\mathbf{q}_2)(d\mathbf{q}_3) \times g(f_0, \beta; \mathbf{q}_1, \mathbf{q}_2, \mathbf{q}_3)\langle \tilde{\psi}(\mathbf{q}_1)\tilde{\psi}(\mathbf{q}_2)\tilde{\psi}(\mathbf{q}_3)\rangle, \quad (28)$$

where $g\ (\beta = 0) = 0$. Even if the one-point PDF of the streamfunction, ψ, had zero skewness (which it does not since in midlatitudes $\psi \sim \Phi/f$), the nonvanishing triple correlations would impart finite skewness to Φ^c. [If one assumes power-law scaling, $\tilde{\psi}(\mathbf{q}) \sim q^{-3}$ and the integral is dominated by the largest scales kept, where asymmetries appear to be largest.] Similarly, nonvanishing higher-order odd correlations of $\mathbf{v}'$, as well as the fact that higher-order even moments in general cannot be factorized into covariances, will contribute corrections to the statistics of the nonlinear terms as derived from a Gaussian model.

Acknowledgments. It is a pleasure to thank G. Boer and F. Zwiers for many useful discussions. S. Lambert

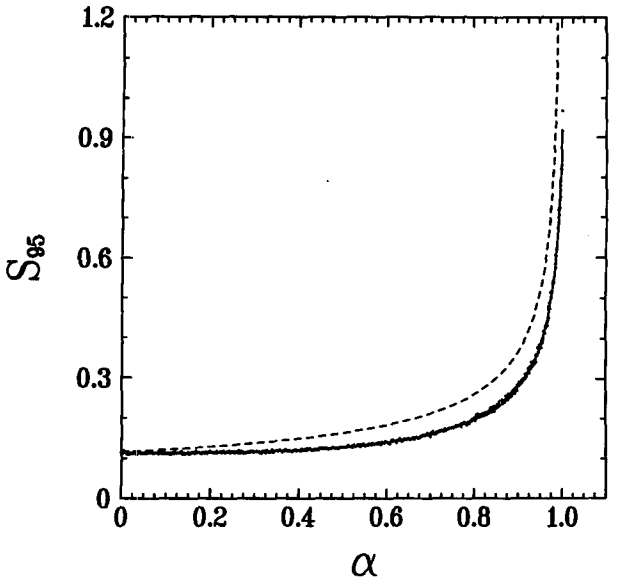

FIG. 13. The threshold for significant skewness at the 5% level, $S_{95}(N_{obs}, \alpha)$, determined numerically from a first-order Markov process of $N_{obs} = 1800$ iterations, plotted (data points) versus lag-one correlation coefficient, α. The solid line is an empirical fit to the data (see text), and the dashed line shows the estimate $2\sqrt{6/(N_{obs}(1-\alpha))}$ for S_{95}.

and J. Fyfe kindly provided the observational data. I thank them, together with N. McFarlane and J. Sheng, for additional helpful discussions. I am grateful to the Atmospheric Environment Service for support administered by the Natural Sciences and Engineering Research Council of Canada.

APPENDIX

Threshold for Statistically Significant Skewness

The skewness computed from (4) for N samples drawn from a symmetric distribution will have a nonzero random sample skewness. The magnitude of this random sample skewness has a probability density function $P_0(|S|, N)$ [with $P_0(|S|, \infty) = \delta(|S|)$], and here we ask the question how large the magnitude of a skewness computed from N_{obs} observations must be so as to be unlikely to come from that distribution. We will consider a skewness to be significantly different at the 5% level from what it would be for a normal distribution, if its magnitude exceeds the 95th percentile, S_{95}, of $P_0(|S|)$. In other words, S_{95} may be taken to be the threshold that $|S|$ computed from real data must exceed to be considered "statistically significant at the 5% level."

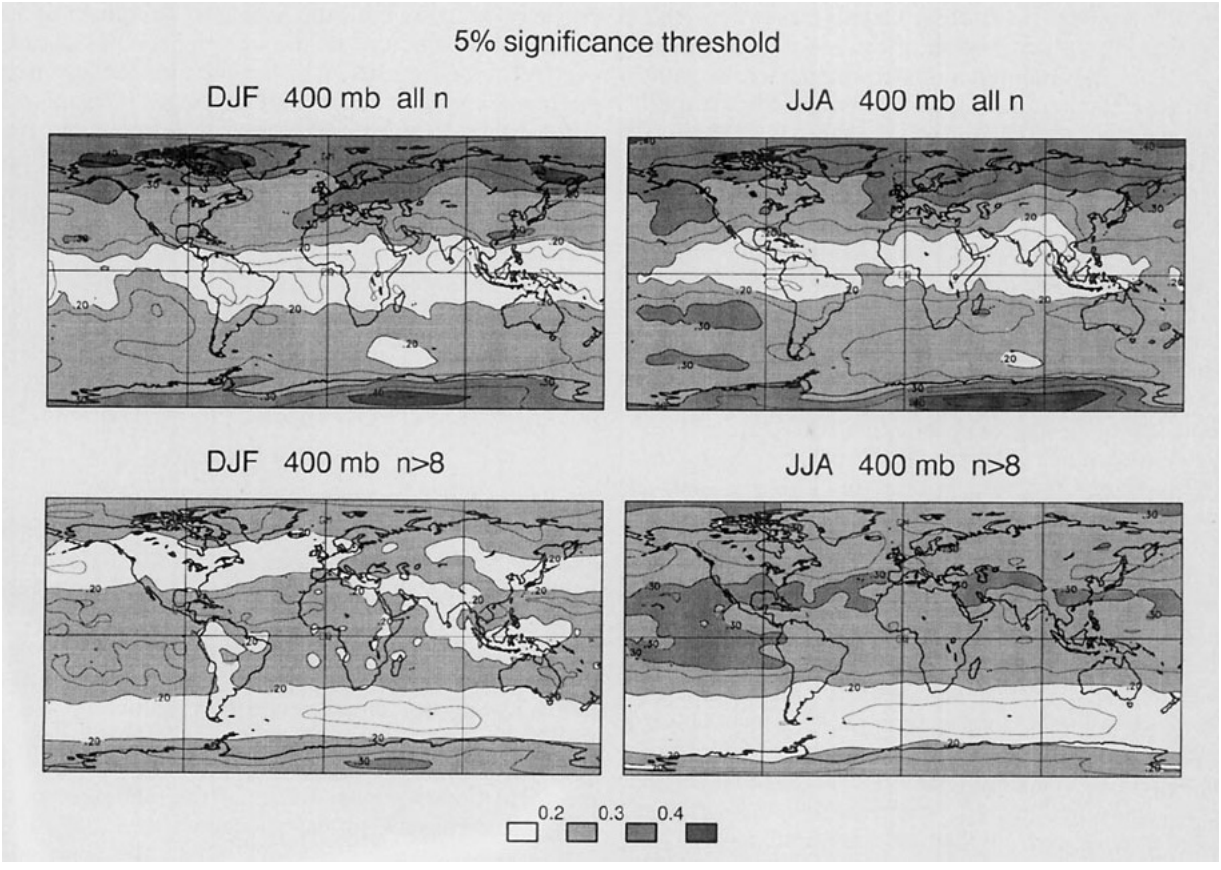

FIG. 14. Maps of the threshold for significant skewness magnitude at the 5% level for the unfiltered and filtered ($n > 8$) geopotential as determined from the lag-one correlation coefficient, α, and the fit to $S_{95}(N_{obs}, \alpha)$ shown in Fig. 13. The contour interval is 0.05.

If the samples are statistically independent and N is large, the answer is quoted in White (1980) and Nakamura and Wallace (1991):

$$S_{95} = 2\sqrt{6/N}. \qquad \text{(A1)}$$

The difficulty here lies in determining the number of independent samples N given a time series of N_{obs} observations taken every $\Delta t = 12$ h, which has serial correlations. For simplicity we will assume here that the consecutive ten winters ($N_{obs} = 1800$) form a (temporally) homogeneous time series. (This will lead to a slight underestimate of the number of independent samples from what it would be if we treated the ten winters as independent.) A simple estimate of N can be obtained from the lag-one correlation coefficient, $\alpha \equiv \langle \Phi'(t)\Phi'(t - \Delta t)\rangle / \langle \Phi'^2(t)\rangle$, of the data as $N = N_{obs}(1 - \alpha)$. This is essentially what was done by Nakamura and Wallace (1991). For our data, the largest correlation coefficients are about $\alpha \sim 0.8$ to 0.9, so that this simple estimate gives $S_{95} \sim 0.26$ to 0.37.

A more consistent, direct estimate that does not require us to guess the number of independent samples can be obtained if we make the assumption that the data has the same statistics as a Gaussian first-order Markov process with a specified lag-one correlation coefficient α. We thus assess statistical significance by comparing the data to the synthetic time series generated by

$$\Phi'(t) = \alpha\Phi'(t - \Delta t) + \eta(t), \qquad \text{(A2)}$$

where the $\eta(t)$ are statistically independent, identically distributed, zero-mean Gaussian random numbers. For this Markov process, the threshold $S_{95}(N_{obs}, \alpha)$ is then easily determined numerically by generating a large number, M, independent length $N_{obs} = 1800$ synthetic time series, and computing their skewnesses. The threshold S_{95} is then approximated by the average of the $(0.95M)$th and the $(0.95M + 1)$th element of the ordered sequence of the skewness magnitudes (see, e.g., Hogg and Tanis 1983).

Figure 13 shows S_{95} thus obtained (with $M = 4000$) as a function of α together with the estimate $2\sqrt{6/(N_{obs}(1 - \alpha))}$. We get an excellent fit to the numerical data for S_{95} by fitting $\log(S_{95})$ to a power series in $\xi \equiv \log(1 - \alpha)$. The fit shown in Fig. 13 is a sixth-order polynomial in ξ that converges rapidly after order ξ^4. This fit was used to transfer maps of α to maps of S_{95} shown in Fig. 14 for 400 mb DJF and JJA, both for the unfiltered and filtered ($n > 8$) data. In the vicinity of the zonal bands of negative skewness (Fig. 1), typically $S_{95} \sim 0.25$. Only for the unfiltered data does S_{95} exceed 0.35, and this occurs in the polar regions well away from the large negative skewness bands of Fig. 1.

REFERENCES

Boer, G. J., 1994: Mean and transient spectral energy and enstrophy budgets. *J. Atmos. Sci.,* **51,** 1765–1779.

——, and T. G. Shepherd, 1983: Large-scale two-dimensional turbulence in the atmosphere. *J. Atmos. Sci.,* **40,** 164–184.

Brachet, M. E., 1991: Direct simulation of three-dimensional turbulence in the Taylor–Green vortex. *Fluid Dyn. Res.,* **8,** 1–8.

Gates, W. L., P. R. Rowntree, and Q.-C. Zeng, 1990: Validation of climate models. *Climate Change, The IPCC Scientific Assessment,* J. T. Houghton, G. J. Jenkins, and J. J. Ephraums, Eds., Cambridge University Press, 93–130.

Haltiner, G. J., and R. T. Williams, 1980: *Numerical Prediction and Dynamic Meteorology.* 2d ed. Wiley and Sons, 477 pp.

Hogg, R. V., and E. A. Tanis, 1983: *Probability and Statistical Inference.* 2d ed. Macmillan, 533 pp.

Holzer, M., and E. Siggia, 1993: Skewed, exponential pressure distributions from Gaussian velocities. *Phys. Fluids,* **A 5,** 2525–2532.

Hosking, J. R. M., 1990: *L*-moments: Analysis and estimation of distributions using linear combinations of order statistics. *J. R. Stat. Soc.,* **52,** 105–124.

Landau, L. D., and E. M. Lifshitz, 1987: *Fluid Mechanics.* 2d ed. Pergamon, 539 pp.

McFarlane, N. A., G. J. Boer, J.-P. Blanchet, and M. Lazare, 1992: The Canadian Climate Centre second-generation general circulation model and its equilibrium climate. *J. Climate,* **5,** 1013–1044.

Nakamura, H., and J. M. Wallace, 1991: Skewness of low-frequency fluctuations in the tropospheric circulation during the Northern Hemisphere winter. *J. Atmos. Sci.,* **48,** 1441–1448.

Siggia, E. D., 1981: Numerical study of small-scale intermittency in three-dimensional turbulence. *J. Fluid Mech.,* **107,** 375–406.

Trenberth, K. E., and J. G. Olson, 1988: Intercomparison of NMC and ECMWF global analyses: 1980–1986. NCAR Tech. Note NCAR/TN-301+STR, 81 pp.

Vautard, R., B. Legras, and M. Déqué, 1988: On the source of midlatitude low-frequency variability. *J. Atmos. Sci.,* **45,** 2811–2843.

von Kármán, T., and L. Howarth, 1938: On the statistical theory of isotropic turbulence. *Proc. Roy. Soc. London,* **164,** 192–215.

White, G. H., 1980: Skewness, kurtosis and extreme values of Northern Hemisphere geopotential heights. *Mon. Wea. Rev.,* **108,** 1446–1455.